REPORT 197

ZIRCON FINGERPRINTING OF MAGMATIC–HYDROTHERMAL SYSTEMS IN THE ARCHEAN YILGARN CRATON

by Y Lu, RH Smithies, MTD Wingate, NJ Evans, TC McCuaig, DC Champion and M Outhwaite

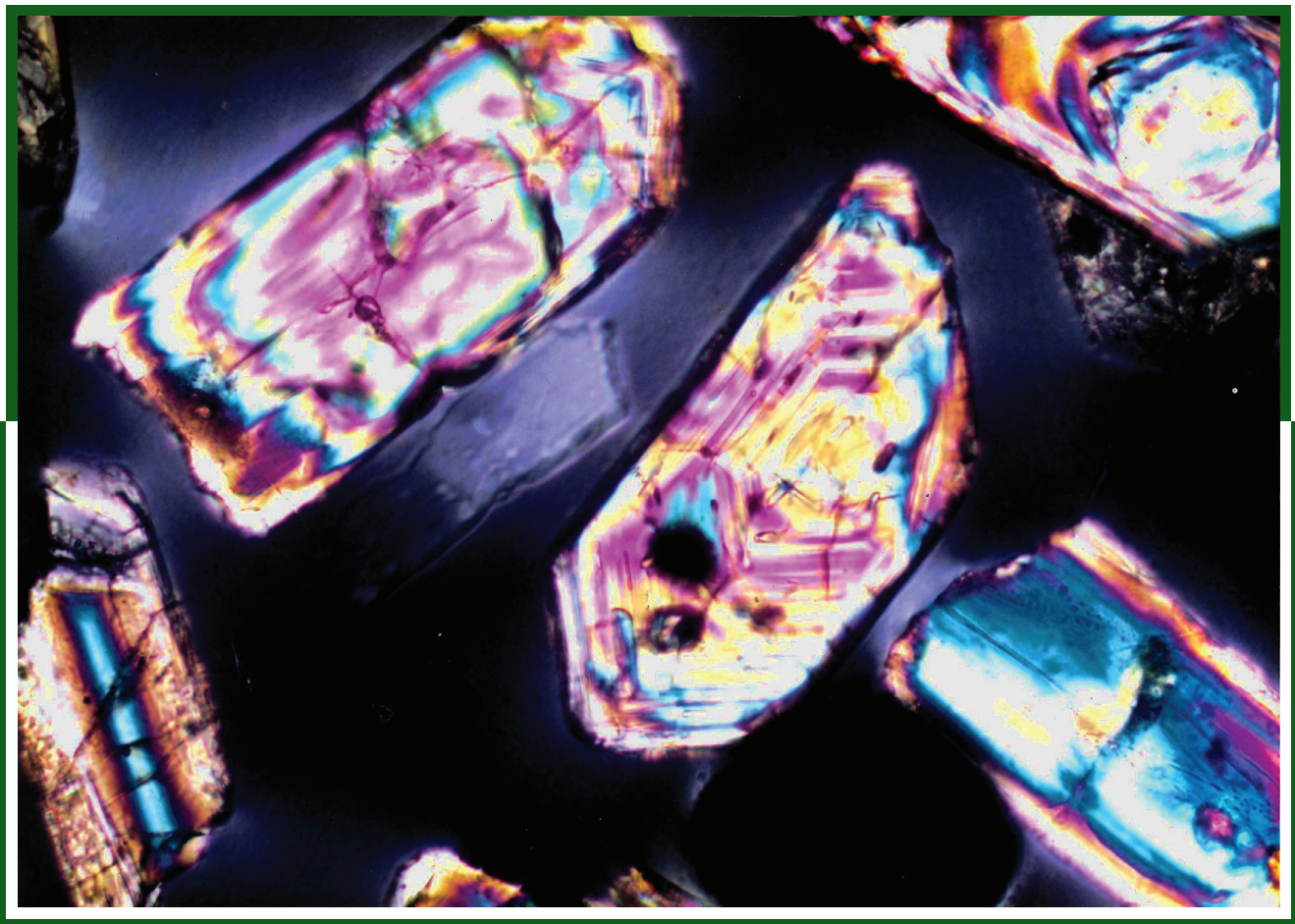

Government of **Western Australia**
Department of **Mines, Industry Regulation and Safety**

Geological Survey of Western Australia

Government of **Western Australia**
Department of **Mines, Industry Regulation and Safety**

REPORT 197

ZIRCON FINGERPRINTING OF MAGMATIC–HYDROTHERMAL SYSTEMS IN THE ARCHEAN YILGARN CRATON

by
Y Lu, RH Smithies, MTD Wingate, NJ Evans[1], TC McCuaig[2], DC Champion[3] and M Outhwaite[4]

1 School of Earth and Planetary Sciences / John de Laeter Centre, Curtin University, Kent Street, Bentley WA 6105
2 BHP, 125 St Georges Terrace, Perth WA 6000
3 Geoscience Australia, GPO Box 378, Canberra ACT 2601
4 Model Earth Pty Ltd, Unit 2, 80 Colin Street, West Perth WA 6005

PERTH 2019

Geological Survey of Western Australia

MINISTER FOR MINES AND PETROLEUM
Hon Bill Johnston MLA

DIRECTOR GENERAL, DEPARTMENT OF MINES, INDUSTRY REGULATION AND SAFETY
David Smith

EXECUTIVE DIRECTOR, GEOLOGICAL SURVEY AND RESOURCE STRATEGY
Jeff Haworth

REFERENCE
The recommended reference for this publication is:
Lu, Y, Smithies, RH, Wingate, MTD, Evans, NJ, McCuaig, TC, Champion, DC and Outhwaite, M 2019, Zircon fingerprinting of magmatic–hydrothermal systems in the Archean Yilgarn Craton: Geological Survey of Western Australia, Report 197, 22p.

ISBN 978-1-74168-864-1
ISSN 1834-2280

A catalogue record for this book is available from the National Library of Australia

Grid references in this publication refer to the Geocentric Datum of Australia 1994 (GDA94). Locations mentioned in the text are referenced using Map Grid Australia (MGA) coordinates, Zone 50. All locations are quoted to at least the nearest 100 m.

About this publication
Zircon U–Pb and trace element compositions were measured using LA-ICP-MS instruments at the GeoHistory Facility, John de Laeter Centre, Curtin University, funded via an Australian Geophysical Observing System grant provided to AuScope Pty Ltd by the AQ44 Australian Education Investment Fund program. Analyses were funded by the Western Australian Government's Exploration Incentive Scheme (EIS). We thank Neal McNaughton for providing zircon samples from the Boddington gold mine, Brad McDonald for technical assistance with LA-ICP-MS analysis, and Paul Morris for assistance with compilation of Yilgarn Craton granitic rocks geochemistry.

Published 2019 by the Geological Survey of Western Australia
This Report is published in digital format (PDF) and is available online at <www.dmp.wa.gov.au/GSWApublications>.

Further details of geoscience publications are available from:
Information Centre
Department of Mines, Industry Regulation and Safety
100 Plain Street
EAST PERTH WESTERN AUSTRALIA 6004
Telephone: +61 8 9222 3459 Facsimile: +61 8 9222 3444
www.dmp.wa.gov.au/GSWApublications

Cover photograph: Separated zircon crystals viewed with crossed polarizers

Contents

Figures

Tables

Zircon fingerprinting of magmatic–hydrothermal systems in the Archean Yilgarn Craton

by

Y Lu, RH Smithies, MTD Wingate, NJ Evans[1], TC McCuaig[2], DC Champion[3] and M Outhwaite[4]

Abstract

Porphyry Cu±Au±Mo deposits throughout the world are mostly Phanerozoic in age and are genetically associated with high-Sr/Y (≥40) granitic rocks. Although these high-Sr/Y granitic rocks dominate Archean terranes, Archean porphyry deposits are extremely rare. The reasons for this have not yet been resolved. Here we compare the zircon trace element content of barren granitic rocks to that of fertile granitic rocks (defined as paragenetically associated with mineralization) from the Calingiri Cu–Mo and Boddington Au–Cu–Mo deposits in the Archean Yilgarn Craton. We compare zircon compositions for Archean granitic rocks with their global Phanerozoic counterparts. Zircons from Archean and Phanerozoic fertile granitic rocks have distinctly high Eu anomaly values (Eu/Eu*>0.4), mainly due to zircons in fertile systems crystallizing from hydrous melts. In addition, Eu/Eu* can be combined with Yb/Gd and Th/U ratios to track the crystallization of different minerals prior to, or concurrent with, zircon crystallization — a process that is not resolvable using whole-rock geochemical data. We propose that the zircon Eu anomaly and trace element ratios can be used to distinguish fertile from barren granitic rocks in Archean and Phanerozoic terranes, providing an effective geochemical exploration tool to assess the fertility of granitic rocks over geological time.

KEYWORDS: Archean, magma fertility, porphyry Cu deposit, Yilgarn Craton, zircon

Introduction

Porphyry Cu±Mo±Au deposits associated with high-Sr/Y (≥40) granitic rocks supply nearly 75% of the world's Cu, about 50% of its Mo, and about 25% of its Au (Sillitoe, 2010). They range in age from Archean to recent, although most are Jurassic or younger (e.g. Cooke et al., 2005; Sinclair, 2007). High-Sr/Y granitic rocks dominate the exposed Archean crust worldwide (Moyen and Martin, 2012), yet Archean porphyry deposits are rare, and the reasons for this remain unclear. Nevertheless, the largest known Au deposits in Australia and Canada, the Boddington and Malartic deposits, respectively, are Neoarchean aged and genetically associated with granitic intrusions. The Boddington deposit in the South West Terrane of the Yilgarn Craton contains more than 720 t of Au and significant quantities of Cu and Mo (McCuaig et al., 2001), whereas the Malartic deposit in the Abitibi greenstone belt of the Superior Craton contains 520 t of Au (Helt et al., 2014). Other Archean porphyry-like deposits include the Calingiri Cu–Mo and Granny Smith Au deposits in the Yilgarn Craton (Mueller et al., 2008; Outhwaite, 2018; Witt et al., 2018), the Hemlo and Lac Bachelor Au deposits in the Superior Craton (Lin and Beakhouse, 2013; Fayol and Jebrak, 2017), Malanjkhand Cu–Mo–Au deposit in the Indian Craton (Stein et al., 2004), and the 3.3 Ga Spinifex Ridge Mo–Cu deposit in the Pilbara Craton, which is the oldest known porphyry deposit in the world (Barley, 1982; Stein et al., 2007).

Archean magmatic–hydrothermal metal deposits are extremely challenging to discover due to widespread weathering, burial by transported cover, deformation and metamorphism in ancient terranes, thus their potential occurrence in Archean cratons may not have been fully recognized. Chemical fingerprinting and/or fertility assessment of granitic intrusions from terrane to deposit scale will help predict potential exploration targets (e.g. Hronsky et al., 2012; Loucks, 2014; McCuaig and Hronsky, 2014; Dilles et al., 2015; Lu et al., 2016; Williamson et al., 2016; Loader et al., 2017). Here we present the first craton-wide study to systematically examine zircons from granitic rocks in the Yilgarn Craton as potential metallogenic fertility indicators of Archean magmatic–hydrothermal systems.

Archean barren and fertile granitic rocks in the Yilgarn Craton

To identify chemical signatures diagnostic of metallogenic fertility in Archean granitic rocks, we have undertaken a systematic study of zircon crystals from both mineralized (fertile; defined as paragenetically associated with

1 School of Earth and Planetary Sciences / John de Laeter Centre, Curtin University, Kent Street, Bentley WA 6105

2 BHP, 125 St Georges Terrace, Perth WA 6000

3 Geoscience Australia, GPO Box 378, Canberra ACT 2601

4 Model Earth Pty Ltd, Unit 2, 80 Colin Street, West Perth WA 6005

mineralization) and unmineralized (barren) granitic rocks in the Yilgarn Craton of Western Australia (Fig. 1). We compiled geochronology and whole-rock geochemistry data for 251 granitic rocks (246 barren and 5 fertile) across the Yilgarn Craton (Fig. 1; Supplementary Table 1). The whole-rock geochemistry of these compiled samples has been published in the Geological Survey of Western Australia's (GSWA) Western Australian Geochemistry database (WACHEM; which can be accessed via GeoChem Extract at <www.dmp.wa.gov.au/launch/geochemistry>). The dataset has been filtered to include only samples with loss on ignition (LOI) values <3.5 wt%, SiO_2 >63 wt% and Al_2O_3 <20 wt% (oxides on an anhydrous basis) to remove samples that are strongly altered or have non-granitic compositions (i.e. mafic to intermediate lithologies and plagioclase cumulates). The barren granitic rocks are divided into four groups (Fig. 2), based on their Sr/Y and K_2O/Na_2O ratios:

- Potassic high-Sr/Y granitic rocks with K_2O/Na_2O ≥1 and Sr/Y ≥40
- Potassic low-Sr/Y granitic rocks with K_2O/Na_2O ≥1 and Sr/Y <40
- Sodic high-Sr/Y granitic rocks with K_2O/Na_2O <1 and Sr/Y ≥40
- Sodic low-Sr/Y granitic rocks with K_2O/Na_2O <1 and Sr/Y <40.

A Sr/Y ratio of 40 is used to distinguish between high- and low-Sr/Y groups because Phanerozoic porphyry Cu deposits are typically associated with granitic rocks that have Sr/Y ≥40 (Chiaradia et al., 2012; Loucks, 2014), and the average Archean tonalite–trondhjemite–granodiorite (TTG) has Sr/Y >40 (Moyen and Martin, 2012). A K_2O/Na_2O ratio of 1 is used to distinguish between potassic and sodic groups. The studied sodic high-Sr/Y granitic rocks in the Yilgarn Craton all have <1.5 ppm Yb, with an average of 0.52 ppm (Supplementary Table 1), and are broadly equivalent to typical Archean TTG series rocks (e.g. Moyen and Martin, 2012).

The fertile granitic rock group includes two granitic rocks from the Calingiri Cu–Mo deposit (with crystallization ages of c. 3010 Ma), and three diorite to dacite porphyry samples from the Boddington Au–Cu–Mo mine (crystallization ages of c. 2700 Ma; McCuaig et al., 2001). We also include two barren, late granite samples (crystallization ages of c. 2670 Ma) that post-date the mineralization event at Calingiri and one late granite (with a crystallization age of c. 2613 Ma) that post-dates mineralization at Boddington for comparison (Supplementary Table 1).

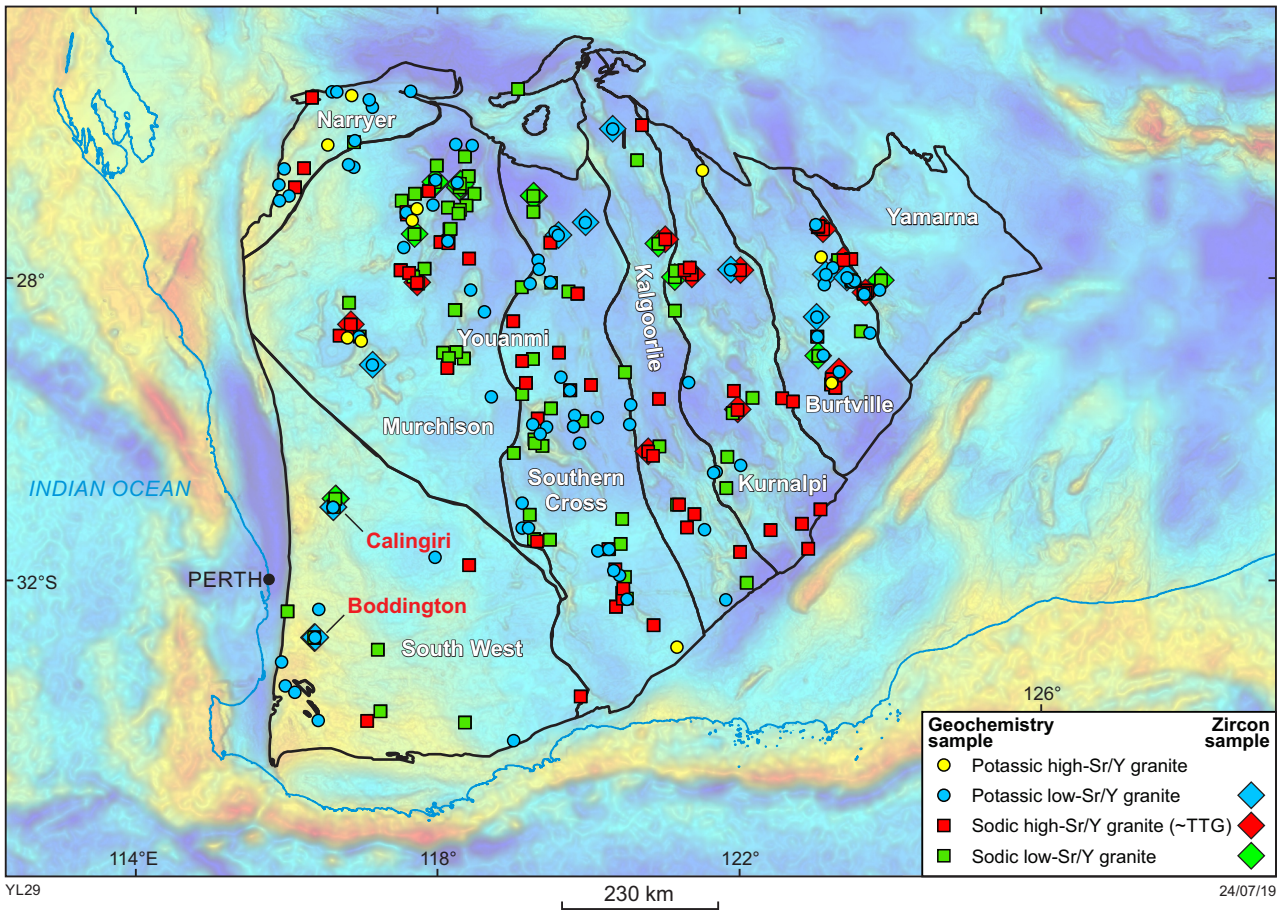

Figure 1. Granitic whole-rock and zircon sample locations superimposed on a gravity image of the Yilgarn Craton (modified after Brett, 2019). Terrane boundaries (black lines) and names are after Pawley et al. (2012). Zircon samples include only those yielding primary trace element data

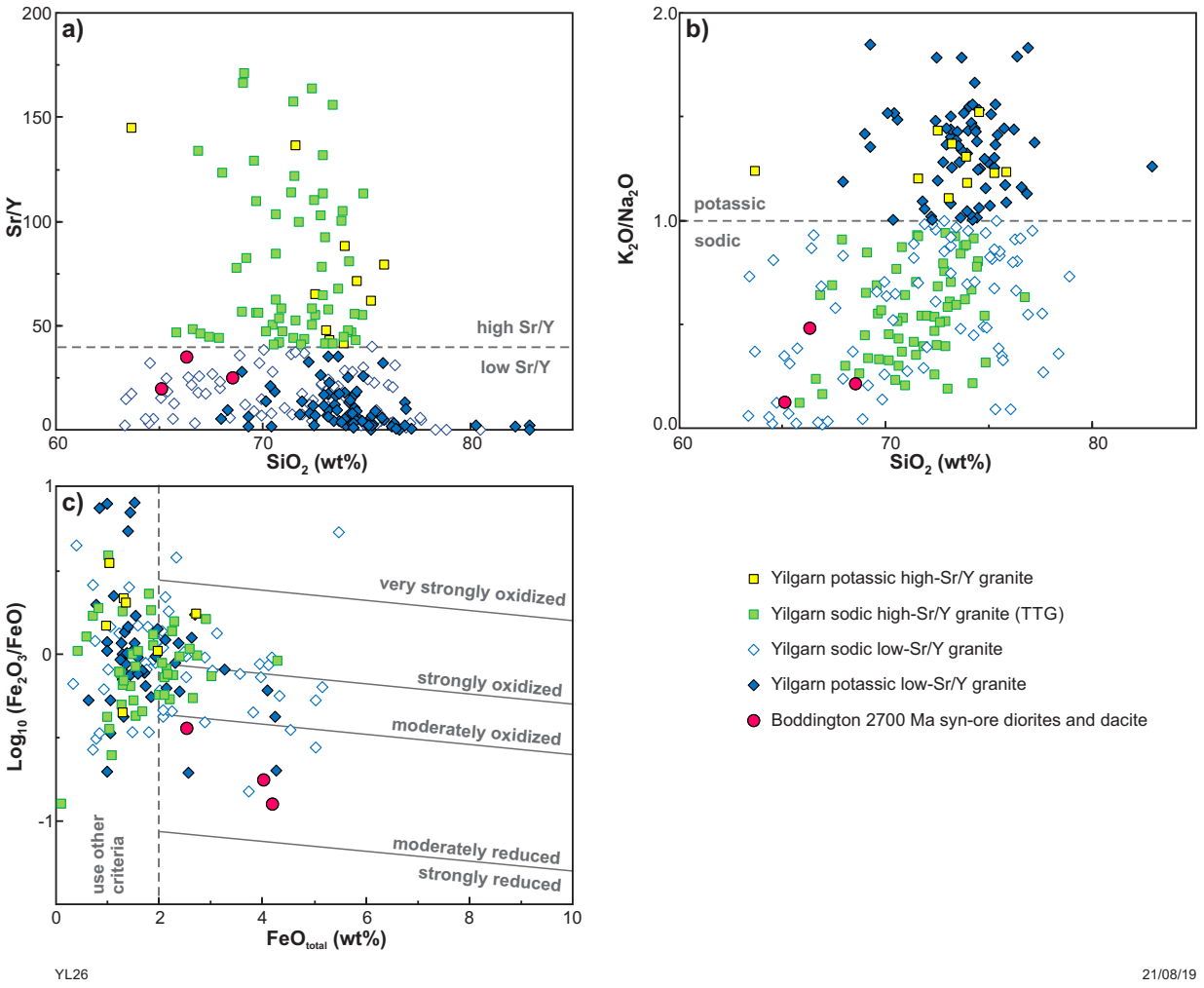

Figure 2. Whole-rock compositions of Archean granitic rocks in the Yilgarn Craton: a) Sr/Y vs SiO_2; b) K_2O/Na_2O vs SiO_2. SiO_2 on anhydrous basis: c) Log_{10} (Fe_2O_3/FeO) vs FeO_{total}. Note that for samples with FeO_{total} <2 wt%, criteria other than whole-rock Fe_2O_3 and FeO data should be used to assess oxidation state (Blevin, 2004). Whole-rock geochemistry data is provided in Supplementary Table 1

Methods

Sample preparation

Zircon samples were selected from rocks that had previously been dated by GSWA using the sensitive high-resolution ion microprobe (SHRIMP; available from <www.dmp.wa.gov.au/geochron>). Zircons were extracted using heavy liquid and magnetic separation techniques. Representative grains were handpicked under a binocular microscope, mounted in epoxy resin disks, then polished to approximately half-grain thickness and coated with Au. The internal structures of zircon crystals were examined using cathodoluminescence (CL) techniques. Details of sample preparation and U–Pb analysis are described in Lu et al. (2019).

Zircon chemistry

The samples were analysed by laser ablation inductively coupled plasma mass spectrometry (LA-ICP-MS) at the John de Laeter Centre, Curtin University, Western Australia. Individual zircons were ablated using a Resonetics RESOlution M-50A-LR sampling system, incorporating a Compex 102 excimer laser. Samples were ablated for 30 s using a 7-Hz repetition rate, 33 µm beam spot and laser energy of 1.5 J/cm^2 (measured at the sample surface). The sample cell was flushed by ultrahigh purity He (680 ml/min) and N_2 (2.8 ml/min). Intensities of isotope peaks were measured using an Agilent 7700s quadrupole ICP-MS, with high-purity Ar as the plasma gas. The masses analysed were: ^{29}Si, ^{31}P, ^{43}Ca, ^{45}Sc, ^{49}Ti, ^{51}V, ^{57}Fe, ^{63}Cu, ^{88}Sr, ^{89}Y, ^{91}Zr, ^{93}Nb, ^{95}Mo, ^{118}Sn, ^{139}La, ^{140}Ce, ^{141}Pr, ^{146}Nd, ^{147}Sm, ^{151}Eu, ^{157}Gd, ^{159}Tb, ^{163}Dy, ^{165}Ho, ^{166}Er, ^{169}Tm, ^{172}Yb, ^{175}Lu, ^{178}Hf, ^{181}Ta, ^{182}W, ^{204}Pb, ^{206}Pb, ^{207}Pb, ^{208}Pb, ^{232}Th and ^{238}U. In each scan of the mass spectrum, the dwell time for most elements was 0.01 s, with the exception of ^{88}Sr (0.02 s), ^{139}La (0.04 s), ^{141}Pr (0.04 s), ^{204}Pb, ^{206}Pb, ^{207}Pb, ^{208}Pb (all Pb 0.03 s each), ^{232}Th (0.0125 s) and ^{238}U (0.0125 s). These settings are generally the same as those in Lu et al. (2016), which reported the zircon compositions of global Phanerozoic fertile and infertile igneous rocks (Fig. 3). Therefore, the new results are comparable with those from global Phanerozoic zircons in Lu et al. (2016). Given the inability to correct for the double-charged ^{90}Zr interference on ^{45}Sc, data for Sc were not used.

International glass standard NIST 610 was used as the primary standard to calculate elemental concentrations and to correct for instrument drift. Secondary standards were analysed after every 15 to 20 unknown samples (i.e. 3–4% of total analyses). Analytical accuracy is estimated to be ±10% (except for Fe, which is ±20%) based on multiple analyses of NIST 612 (secondary standard; Jochum et al., 2005), whereas analytical precision (coefficient of variation) was better than ±4% for most elements.

Intersecting small mineral inclusions at depth in an ablation pit is common in LA-ICP-MS analysis of zircons. We used the criteria proposed by Lu et al. (2016) to systematically exclude analyses contaminated by inclusions: La >1 ppm is taken to reflect apatite contamination, which is the most commonly recognized contaminant in zircon; Fe >5000 ppm reflects contamination by Fe oxides; Ti >50 ppm indicates contamination by Ti-(Fe-)-oxides. Ca >500 ppm also suggests inclusion contamination such as feldspar (Burnham and Berry, 2017). We also applied the Light Rare Earth Element Index (LREE-I = [Dy/Nd]+[Dy/Sm]) proposed by Bell et al. (2016), who considered analyses with LREE-I <10 to be clearly altered and those with LREE-I between 10 and 30 to be uncertain, whereas LREE-I >30 indicates primary zircons that have not undergone contamination or hydrothermal alteration. No common-Pb corrections were performed on the U–Pb isotope ratios, and analyses with age discordance >10% were excluded (discordance [%] = 100 × [(^{207}Pb/^{206}Pb date) – (^{238}U/^{206}Pb date)] / [^{207}Pb/^{206}Pb date]; Lu et al., 2019). Zircons that were excluded commonly failed more than one of the criteria above. Dates based on ^{207}Pb/^{206}Pb ratios for compositions <10% discordant were used to identify and exclude xenocrystic zircons or inherited zircon cores. After excluding contaminated zircon signals and xenocrysts, only data relating to magmatic zircons free of contamination are plotted and discussed in the text. All analyzed zircon data are reported in Supplementary Table 2, and the primary zircon data are reported in Supplementary Table 3.

Geochronology

The primary reference material used for U–Pb dating in this study was zircon standard GJ-1 (601.7 ± 1.4 Ma; Jackson et al., 2004; Kylander-Clark et al., 2013), with secondary standard zircons 91500 (1062.4 ± 0.4 Ma; Wiedenbeck et al., 1995) and OGC1 (3465.4 ± 0.6 Ma; Stern et al., 2009). OGC1 is the zircon standard obtained by Curtin University from the same rock from that standard OG1 was described by Stern et al. (2009). The ^{207}Pb/^{206}Pb ages of the OGC1 standard were used to check the accuracy of dated samples and all fall within uncertainty of the accepted value. For example, the weighted mean ^{207}Pb/^{206}Pb age determined for OGC1 across all runs was 3468 ± 5 Ma (n = 60, MSWD = 1.4), consistent with the recommended value within uncertainty (3465 Ma; Stern et al., 2009). Time-resolved mass spectra were reduced using the U_Pb_Geochronology4 and Trace_Elements_IS data reduction schemes in Iolite (Paton et al., 2011, and references therein).

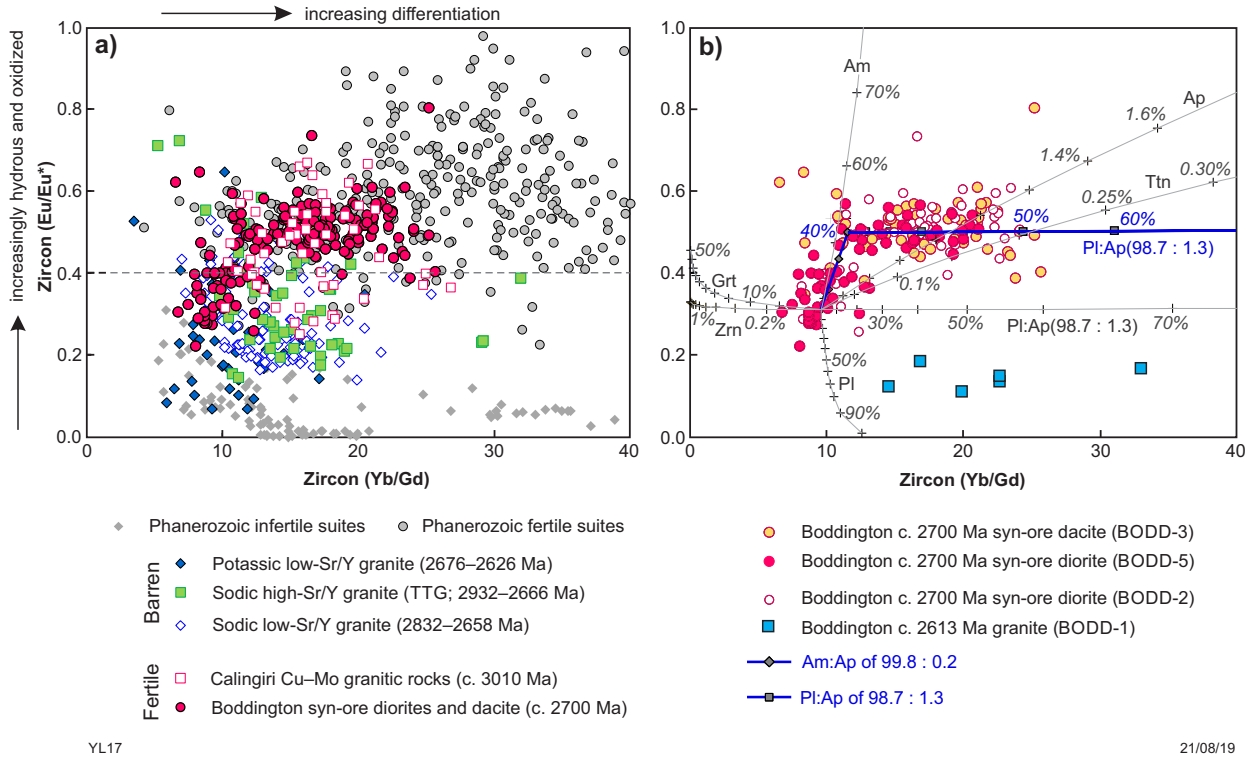

Figure 3. Zircon Eu/Eu* vs Yb/Gd ratios: a) all primary magmatic zircon analyses from Archean fertile and barren granitic rocks in the Yilgarn Craton (Supplementary Table 3) and global Phanerozoic fertile and infertile igneous rocks (Lu et al., 2016); b) four individual samples from Boddington Au mine showing within-sample variation and Rayleigh fractionation modelling curves of various minerals, with the numbers indicating percentage of crystallization of the related mineral or mineral assemblage. Refer to the text for modelling details. Abbreviations: Am, amphibole; Ap, apatite; Grt, garnet; Pl, plagioclase; Ttn, titanite; Zrn, zircon

Results

Individual zircon crystals were analysed by LA-ICP-MS for U–Pb age and 33 trace elements. The complete results of 2612 zircon analyses for 50 representative granitic rocks samples from across the Yilgarn Craton are reported in Supplementary Table 2. Screening for the effects of alteration and mineral inclusion contamination leaves 458 primary zircon analyses (Supplementary Table 3), which is about four times the amount of published primary zircon data for Archean granitic rocks globally. This new primary zircon chemistry dataset includes chemical compositions of:

- 201 magmatic zircons from 30 regional barren granitic rocks, including sodic high-Sr/Y granitic rocks (TTGs), sodic low-Sr/Y granitic rocks, and potassic low-Sr/Y granitic rocks (no primary data was obtained from potassic high-Sr/Y granitic rocks)
- 233 magmatic zircons from six granitic rocks from the Calingiri and Boddington deposits
- 24 analyses of xenocrystic zircons (not plotted or discussed).

Summary statistics of primary igneous zircon compositions for these samples are included in Table 1, and presented in Figures 3–6.

Rayleigh fractionation model

Zircon compositions are strongly influenced by the prior or concurrent crystallization of other rare earth element (REE)-bearing phases (Burnham and Berry, 2012; Burnham et al., 2015; Smythe and Brenan, 2015; Loader et al., 2017). To illustrate the geochemical impact of minerals crystallized prior to or concurrent with zircon crystallization, we present the Rayleigh fractionation model of single minerals and mineral assemblages following the approach of Loader et al. (2017).

Calculation of model partition coefficients

Partition coefficients (K_d) were selected from the GERM database (http://earthref.org/GERM). The following K_d values (Fig. 7; Table 2) were used: titanite (Bachmann et al., 2005), plagioclase (Dunn and Senn, 1994), zircon and apatite (Sano et al., 2002), amphibole (Klein et al., 1997) and garnet (Burnham and Berry, 2017). The Boddington diorite sample (BODD-2) whole-rock value was used as the starting composition (Table 2).

Rayleigh fractionation of single mineral model

Rayleigh fractionation of a single mineral, such as amphibole, apatite, titanite, plagioclase, zircon and garnet, was calculated using the following formula (Loader et al., 2017):

$$C_l = C_l^0 * F^{(K_{d\,m}-1)}$$

where C_l is the concentration of an element in the liquid, C_l^0 is the initial element concentration in the melt, F is the fraction of melt remaining, and $K_{d\,m}$ is the partition coefficient of a specific mineral above. For example, in the case of the amphibole fractionation model (where only amphibole crystallization from BODD-2 composition was considered), this was done for melt fractions from 1 to 0.01 (i.e. 0–99% amphibole crystallization), in increments of 10%. Zircon in equilibrium with these hypothetical melts was calculated. The results of the fractionation model of amphibole, apatite, titanite, plagioclase, zircon and garnet are presented in Tables 3–8 and illustrated in Figures 3 and 4.

Rayleigh fractionation of amphibole:apatite and plagioclase:apatite model

Rayleigh fractionation of plagioclase:apatite and amphibole:apatite mineral assemblages was calculated using the following formula (Loader et al., 2017):

$$C_l = C_l^0 * F^{(K_{d\,bulk}-1)}$$

where C_l is the concentration of an element in the liquid, C_l^0 is the initial element concentration in the melt, F is the fraction of melt remaining, and $K_{d\,bulk}$ is the bulk partition coefficient.

Bulk K_d values of the plagioclase:apatite and amphibole:apatite assemblages were calculated using:

$$K_{d\,bulk} = (D_a^m * X_m) + (D_a^{ap} * X_{ap})$$

where D_a^m and D_a^{ap} are the partition coefficients for element a in phase m (plagioclase or amphibole) and apatite (ap), and X is the fraction of each phase individually.

The fractionation of amphibole:apatite (99.8 : 0.2) was modelled using sample BODD-2 as a starting composition and the results are presented in Table 9 and illustrated in Figure 3.

Two plagioclase:apatite (98.7 : 1.3) fractionations were modelled, using two starting compositions: 1) model melt after 40% crystallization of amphibole:apatite (99.8 : 0.2) in Table 9; and 2) sample BODD-2. The model results are presented in Tables 10 and 11, respectively, and illustrated in Figures 3 and 4.

Eu/Eu* in zircon: a discriminant between barren and fertile Archean granitic rocks

Europium anomaly (Eu/Eu*) values in zircon are shown in Figures 3–5. The fertile Boddington and Calingiri granitic rocks have higher zircon Eu/Eu* (>0.4 in ~80% of zircons with a median of 0.49 for Boddington and 0.47 for Calingiri) than barren Yilgarn granitic rocks with Eu/Eu* >0.4 only in about 10% in zircons from barren sodic

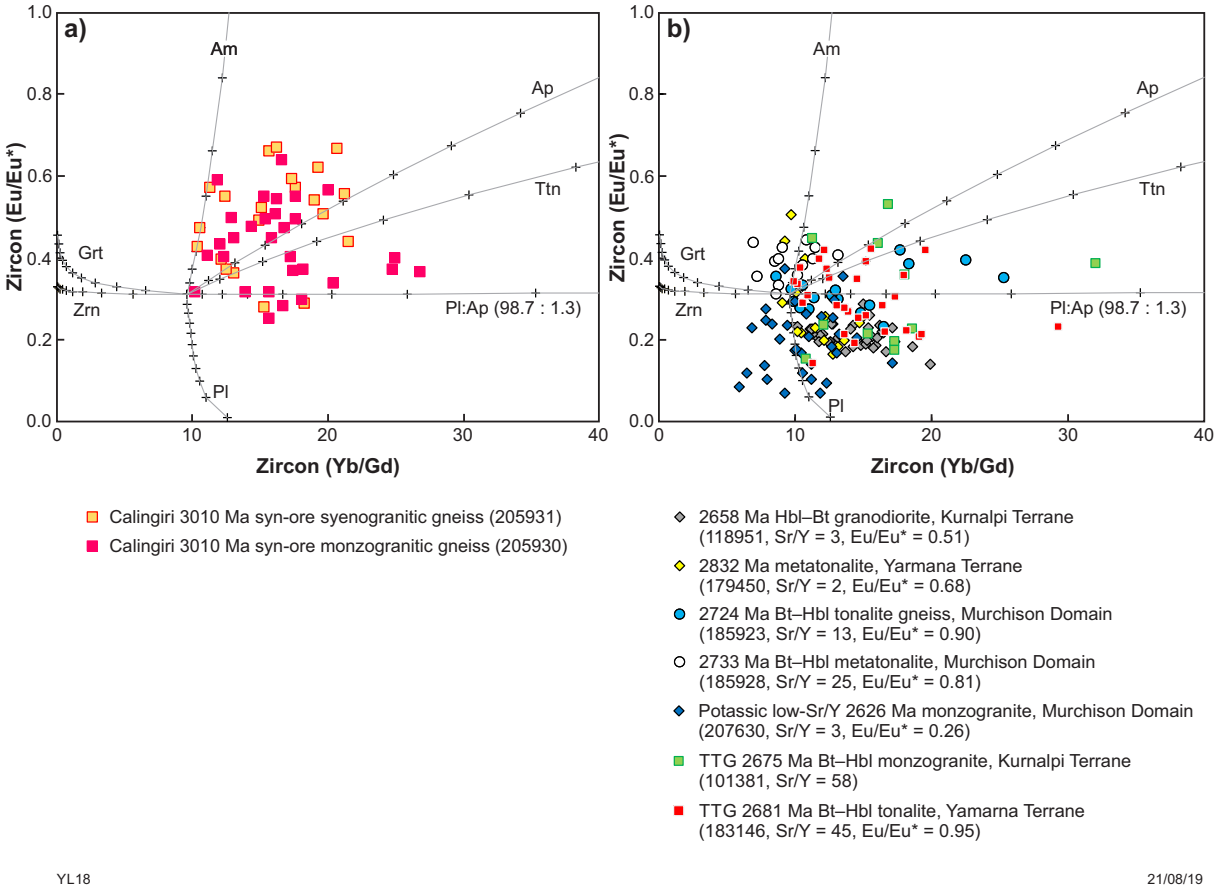

Figure 4. **Zircon Eu/Eu* vs Yb/Gd ratios: a) two mineralized samples from Calingiri Cu–Mo granitic rocks; b) seven individual samples from regional barren Yilgarn Craton granitic rocks with only samples yielding more than 10 primary zircon analyses plotted. Rayleigh fractionation modelling curves and abbreviations are the same as in Figure 3. Abbreviations: Bt, biotite; Hbl, hornblende**

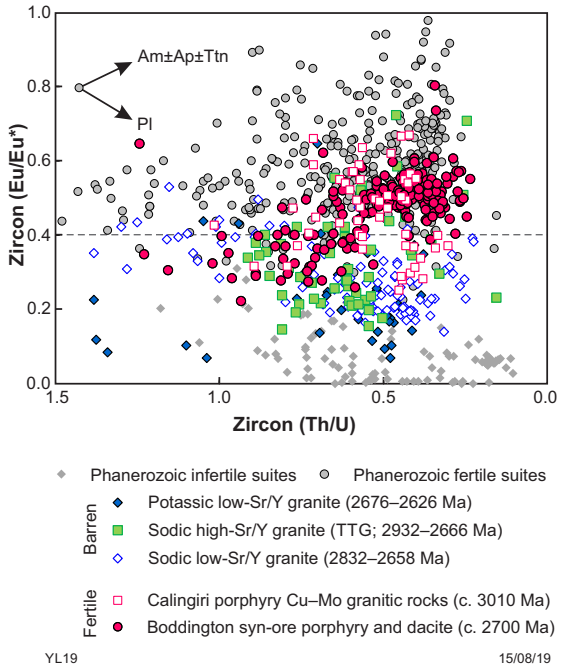

Figure 5. **Zircon Eu/Eu* vs Th/U ratios, with decreasing Th/U indicating increasing differentiation. The schematic vectors showing effect of crystallization of plagioclase and amphibole±apatite±titanite. Data source is the same as in Figure 3**

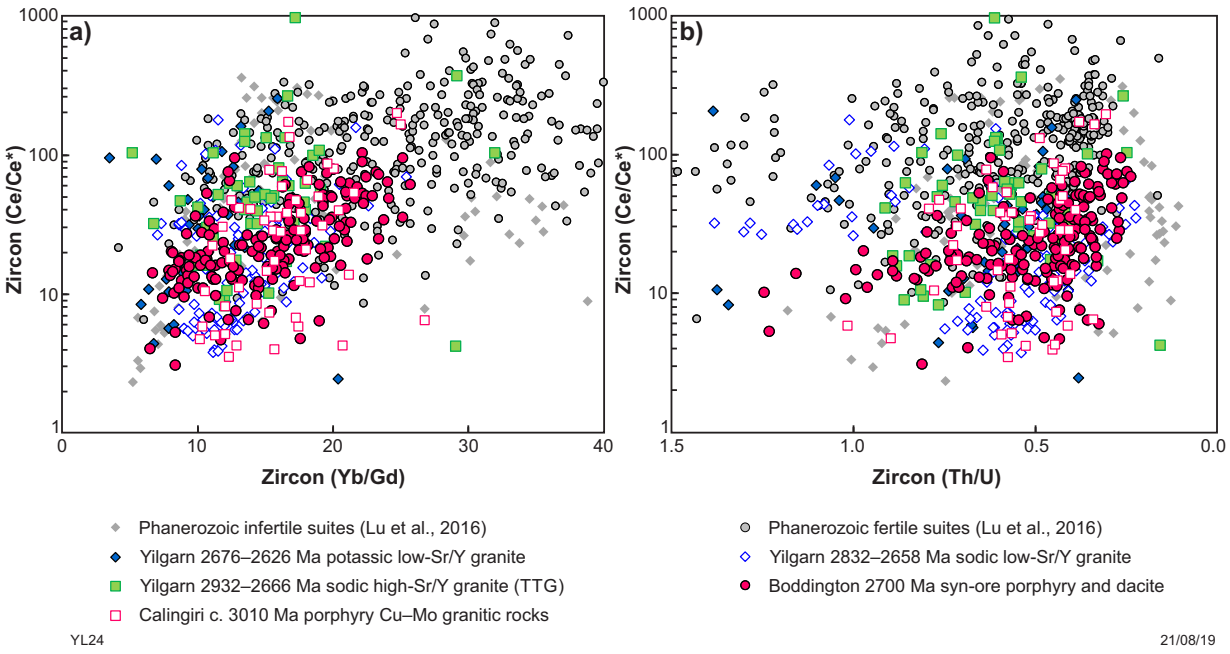

Figure 6. Zircon Ce/Ce* ratios of Archean granitic rocks in the Yilgarn Craton: a) Ce/Ce* vs Yb/Gd; b) Ce/Ce* vs Th/U. Data source is the same as in Figure 3

and potassic low-Sr/Y granitic rocks, and 25% in zircons from sodic high-Sr/Y granitic rocks (TTGs). The median zircon Eu/Eu* is 0.23 for potassic low-Sr/Y granitic rocks, 0.27 for sodic low-Sr/Y granitic rocks and 0.31 for sodic high-Sr/Y granitic rocks (Table 1). This difference is evident across the full age range of Yilgarn granitic rocks from 3.0 to 2.6 Ga (Figs 3, 4). Thus, Eu/Eu* in zircon is an effective discriminant between zircons from fertile and barren Yilgarn granitic rocks.

High Eu/Eu* (>0.4) in zircon has also been reported for Phanerozoic porphyry Cu deposits associated with hydrous and oxidized granitic rocks, typically in convergent margin settings (Fig. 3; Ballard et al., 2002; Dilles et al., 2015; Lu et al., 2016, Lee et al., 2017; Loader et al., 2017; Large et al., 2018). The global Phanerozoic fertile and infertile granitic rocks suites reported by Lu et al. (2016) are plotted for comparison (Figs 3, 5, 6). The Phanerozoic infertile suites are relatively reduced and dry S-, A-, and I-type magmatic rocks, including the Yellowstone rhyolite (Wyoming), Bandelier rhyolite (New Mexico), Bishop tuff rhyolite (California), Lucerne reduced granite (Maine), and Hawkins S-type dacite and Kadoona I-type dacite (Lachlan belt, Australia). The Phanerozoic fertile suites are more oxidized and hydrous I-type intrusions from porphyry and high-sulfidation epithermal Cu–Au deposits (Batu Hijau, Indonesia and Tampakan, Philippines), porphyry Cu–Mo–Au deposits (Sar Cheshmeh, Iran; Dexing, eastern China; and Jiama, southern Tibet), porphyry Cu–Mo deposits (Sungun, Iran and Qulong, southern Tibet) and porphyry Mo deposits (Nannihu and Yuchiling, central China).

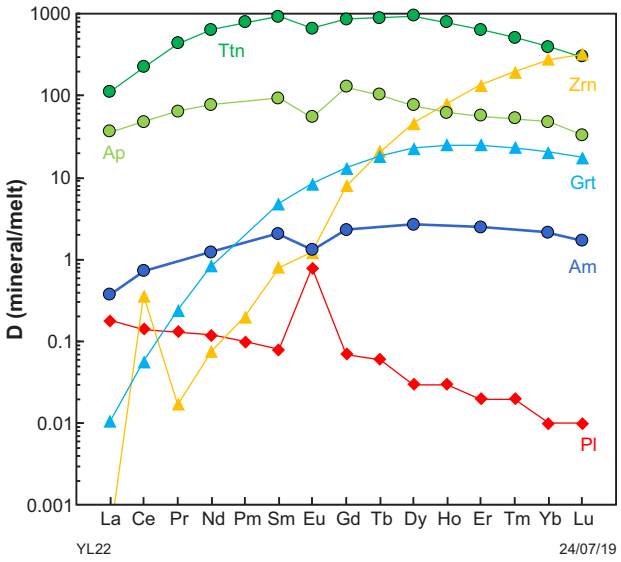

Figure 7. Partition coefficients of REE between mineral and melt. Values are provided in Table 2. Data sources: titanite (Bachmann et al., 2005); plagioclase (Dunn and Senn, 1994); zircon and apatite (Sano et al., 2002); amphibole (Klein et al., 1997); garnet (Burnham and Berry, 2017)

Magmatic redox state can strongly influence the partitioning of Eu in zircon because Eu^{3+} (the oxidized Eu) has a smaller ionic radius than Eu^{2+} (the reduced Eu), therefore making it more compatible in zircon's crystallographic structure. In felsic melts, at typical melt fO_2 and zircon saturation temperatures (750°C; at the fayalite–magnetite–quartz [FMQ] buffer), the $Eu^{3+}/(Eu^{3+} + Eu^{2+})$ ratio reduces to very low values (~0.5; Burnham and Berry, 2014; Burnham et al., 2015), which causes Eu to be less compatible in zircon. Therefore, zircons commonly display negative Eu anomalies (Fig. 7). Based on whole-rock Fe_2O_3/FeO ratios (Blevin, 2004), the Boddington samples are moderately reduced despite their high zircon Eu/Eu* values, whereas barren high- and low-Sr/Y granitic rocks are typically moderately to strongly oxidized (Fig. 2c). Therefore, magmatic redox state alone cannot explain the distinct difference in Eu/Eu* between fertile and barren granitic rocks.

Zircon Eu/Eu* is also influenced by the prior or concurrent crystallization of other REE-bearing phases, which may increase or decrease the Eu/Eu* value of the melt (Burnham and Berry, 2012; Burnham et al., 2015; Smythe and Brenan, 2015; Loader et al., 2017). Among the minerals commonly crystallized before or during zircon saturation in granitic rocks, plagioclase is the only one that preferentially incorporates Eu, with a partition coefficient an order of magnitude higher than the neighbouring REE (Fig. 7; Dunn and Sen, 1994). Thus, crystallization of plagioclase prior to, or during zircon saturation, or retention of plagioclase in the granitic rocks source region, would deplete the melt in Eu, generating a negative Eu anomaly, which would then be inherited by subsequently crystallizing zircons (Table 6; Smythe and Brenan, 2015). In contrast, the partition coefficient of Eu in amphibole, apatite and titanite is lower than that of neighbouring REE, and crystallization of these minerals will increase the melt Eu/Eu* (Fig. 7 and Tables 3–5; Klein et al., 1997; Sano et al., 2002; Bachmann et al., 2005; Loader et al., 2017).

Zircon Yb/Gd, Th/U and Hf concentration are differentiation proxies because Yb/Gd and Hf increase and Th/U decreases with decreasing temperature and high-resolution TIMS ages (Claiborne et al., 2010; Dilles et al., 2015; Lee et al., 2017; Loader et al., 2017; Samperton et al., 2017; Large et al., 2018). On a Eu/Eu* vs Yb/Gd plot, the Boddington c. 2700 Ma zircons display a distinct differentiation trend, with Eu/Eu* increasing from 0.3 to 0.5 with increasing Yb/Gd from 10 to 12, followed by broadly constant Eu/Eu* of 0.5, with increasing Yb/Gd from 12 to 25 (Fig. 3a). Although prior or concurrent titanite crystallization will lead to elevated Eu/Eu* and low Ta contents (<0.2 ppm) in zircon (Loader et al., 2017), igneous titanite is absent from Boddington fertile intrusions and 95% of Boddington zircons have high Ta contents (>0.2 ppm; Supplementary Table 3). This suggests it is unlikely that titanite played a role in the compositional evolution of the Boddington zircons. Given the ubiquitous presence of amphibole, apatite and plagioclase in c. 2700 Ma Boddington samples, genesis of the c. 2700 Ma Boddington diorite–dacites can be best modelled by Rayleigh fractional crystallization of a melt represented by Boddington sample BODD-2; first involving 40% crystallization of an amphibole:apatite (99.8 : 0.2) assemblage, followed by up to 50% crystallization of a plagioclase:apatite (98.7 : 1.3) assemblage (Fig. 3b). This modelling is consistent with crystallization experiments of hydrous andesite with initial 6 wt% water, which can crystallize 30% amphibole in equilibrium with a dacitic residual melt with 12 wt% water at 0.8 GPa and 800°C (Alonso-Perez et al., 2009). Crystallization of amphibole before plagioclase indicates very hydrous melts (>6 wt% water) at elevated pressures (Naney, 1983; Moore and Carmichael, 1998; Loucks, 2014; Lu et al., 2015). Therefore, the c. 2700 Ma fertile granitic rocks at Boddington are best explained by derivation from hydrous melts with high zircon Eu/Eu* (>0.4), attributed to early amphibole-dominated fractionation. In contrast, the c. 2613 Ma barren granite from Boddington has distinctly lower zircon Eu/Eu* (median = 0.14) and a trend suggesting plagioclase- and apatite-dominated fractionation (Fig. 3b). This feature is consistent with the interpretation that the c. 2613 Ma barren Boddington granite was formed by melting of mid-crustal rocks in an intraplate setting, whereas the c. 2700 Ma fertile granitic rocks were likely emplaced into an island arc setting (McCuaig et al., 2001).

The c. 3010 Ma Calingiri fertile granitic rocks (whole-rock Eu/Eu* = 0.93 – 1.08; Supplementary Table 1) have highly variable zircon Eu/Eu* values at any given Yb/Gd ratio (e.g. at Yb/Gd of 15, Eu/Eu* varies from 0.3 to 0.7; Fig. 4a). High and variable Eu/Eu* in zircon is also reported in Phanerozoic porphyry Cu deposits such as El Abra and Chuquicamata (Chile), Yanacocha (Peru), Batu Hijau (Indonesia), Tampakan (Philippines), Dexing (China) and Sungun (Iran), although the origin of this characteristic is still contested (Dilles et al., 2015; Lu et al., 2016). Our Rayleigh fractionation modelling suggests it is likely related to varying degrees and proportions of amphibole, apatite, titanite and plagioclase crystallization (Fig. 4a). On a Eu/Eu* vs Th/U plot (Fig. 5), Calingiri zircons display a broadly increasing Eu/Eu* (from 0.3 to 0.7) with decreasing Th/U (from 1 to 0.5, reflecting increasing differentiation), followed by decreasing Eu/Eu* (from 0.7 to 0.3) when Th/U decreases below 0.5. A similar broad trend is observed in Boddington zircons and Phanerozoic porphyry Cu deposits, consistent with early differentiation dominated by amphibole, apatite and titanite, and late differentiation dominated by plagioclase in fertile magmas (Fig. 5). The two barren post-ore c. 2670 Ma granitic rocks (whole-rock Eu/Eu* = 0.57 – 0.65; Supplementary Table 1) from Calingiri do not yield primary magmatic zircon analyses due to ubiquitous inclusion contamination. However, their zircon Eu/Eu* may be estimated to be ~0.3, because Eu/Eu* values in zircon are typically about 0.48 × whole-rock Eu/Eu* (assuming zircons are in equilibrium with the whole-rock composition; see Rayleigh fractional crystallization modelling results in Tables 3–11).

Plagioclase crystallization controls the compositional evolution of zircon in barren Yilgarn potassic and sodic low-Sr/Y granitic rocks and sodic high-Sr/Y granitic rocks (TTGs), evidenced by decreasing zircon Eu/Eu* with increasing Yb/Gd and decreasing Th/U. The distinct compositional trends suggest these barren granitic rocks are less hydrous than fertile granitic rocks (Figs 4b, 5). However, about 25% of the zircons from sodic high-Sr/Y granitic rocks (TTGs) display Eu/Eu* >0.4, which increases with decreasing Th/U and suggests that at least some TTGs may have experienced differentiation of amphibole, apatite and titanite (Fig. 5).

The Ce anomaly in zircon (Ce/Ce*) has previously been proposed to distinguish between fertile and barren granitic rocks (e.g. Ballard et al., 2002). The zircon Ce/Ce* is sensitive to magmatic oxidation state and temperature (Burnham and Berry, 2012, 2014; Loucks et al., 2018). However, our comprehensive data show that it is not very effective in discriminating fertile from barren granitic rocks, as shown by significant overlap between fertile and barren samples in both Archean and Phanerozoic systems (Fig. 6). This is probably because, in natural systems, oxygen fugacity and water contents have the opposite effect on Ce/Ce* (high oxidation state will increase Ce/Ce* but high water content will decrease Ce/Ce*; Smythe and Brenan, 2015, 2016).

Implications for exploration

Magma fertility is highly dependent on water content, sulfur content and oxidation state (Rohrlach and Loucks, 2005; Richards, 2011; Loucks, 2014). High water content is the primary control on magma fertility and determines whether or not a magmatic–hydrothermal metal system can form. Hydrous magmas can exsolve a water-rich volatile phase during upper-crustal emplacement, a requirement for formation of an ore system (Burnham, 1979; Richards, 2011). The oxidation state and sulfur content of the magma are secondary to the requirement for sufficient water, although they may influence the metal ratios and endowment (Richards, 2011). The distinctly high zircon Eu/Eu* (>0.4) in fertile granitic rocks is a function of early amphibole crystallization, which confirms their hydrous nature (Fig. 3a).

Because zircon can survive intense hydrothermal alteration, weathering, metamorphism and long-distance detrital transport, it can be used as an indicator for Au–Cu–Mo fertility in weathered and metamorphosed terranes. Previous work has indicated that zircon chemistry is an effective prospectivity tool in Phanerozoic terranes (Ballard et al., 2002; Dilles et al., 2015; Lu et al., 2016) and the results of this study confirm similar potential for prospectivity analysis in Archean terranes. Furthermore, we envisage the use of detrital zircon chemistry from sedimentary rocks as a regional exploration tool for magmatic–hydrothermal metal deposits in Archean terranes, with the potential to identify fertile granitic rocks over large detrital source areas.

Implications for Archean geodynamics

These results not only provide a new exploration tool for Archean magmatic–hydrothermal systems, but also have implications for models of the evolution of Archean crust. Specifically, the results provide a means for determining whether the parental melts of granitic rocks have undergone a water-enriching process, which in turn indicates particular geodynamic settings. For example, Phanerozoic porphyry systems are derived via high-pressure melting and fractionation above subducting oceanic crust in convergent settings (Loucks, 2014). This tectonic process increases water content in the melt. Hence, it may be that fertile Archean granitic rocks, with similar compositional characteristics, also formed in subduction settings. Indeed, the c. 2700 Ma intrusive and volcanic rocks (diorite–andesite–dacite) at the Boddington Au mine have previously been interpreted as having been emplaced in an island arc setting (McCuaig et al., 2001), which is supported by our Boddington zircon Eu/Eu* results (Fig. 3).

Comprehensive trace element data sets for Precambrian zircons are scarce (Burnham and Berry, 2017). The Hadean (4.02 Ga) Idiwhaa tonalitic gneiss of the Acasta Gneiss Complex (Canada) is the oldest intact terrestrial rock unit, and yielded very low zircon Eu/Eu* values (median = 0.18, n = 16; Reimink et al., 2014), consistent with their generation in a non-subduction setting, such as in an Iceland-like setting (Reimink et al., 2014) or via meteorite impact melting (Johnson et al., 2018). The 4.4 – 3.3 Ga detrital zircons from the Jack Hills in Western Australia, which include the oldest known mineral grains on Earth, also yielded low zircon Eu/Eu* values, with 92% of zircons having Eu/Eu* <0.4 (median = 0.19, n = 258; Bell et al., 2016). In contrast, the limited available zircon compositions from 2.7 Ga TTGs and sanukitoid rocks from the Superior Craton exhibit higher zircon Eu/Eu* values (median of 0.59 for TTGs, n = 13 and 0.52 for sanukitoids, n = 18; Bouvier et al., 2012) indicating a hydrous, amphibole-rich parent melt, which is consistent with a subduction-related origin (Percival et al., 2006). However, a systematic study of zircon compositions from the Superior Craton is required to fully test this possibility.

Conclusions

This Report documents the first craton-wide study to systematically examine zircons from granitic rocks in the Archean Yilgarn Craton as potential metallogenic fertility indicators of Archean magmatic–hydrothermal systems. The fertile granitic rocks from the Calingiri Cu–Mo and Boddington Au–Cu–Mo deposits in the Yilgarn Craton show distinctly higher zircon Eu anomaly values (>0.4) and amphibole-dominated fractionation in hydrous melts, similar to Phanerozoic fertile granitic rocks. By contrast, the barren granitic rocks from across the Yilgarn Craton display lower zircon Eu/Eu* values (<0.4) and plagioclase-dominated fractionation. These results suggest that the zircon Eu anomaly and trace element ratios can be used to distinguish fertile from barren granitic rocks in Archean and Phanerozoic terranes, providing an effective geochemical exploration tool to assess the metallogenic fertility of granitic rocks over geological time.

Table 1. Summary statistics of primary igneous zircon geochemistry from Archean granitic rocks of the Yilgarn Craton

Suite	*Sodic low-Sr/Y granite (n = 107)*			*Sodic high-Sr/Y granite (n = 52)*			*Potassic low-Sr/Y granite (n = 41)*			*Calingiri fertile granite (n = 51)*			*Boddington fertile granite (n = 176)*			*Phanerozoic fertile granite (n = 337)*			*Phanerozoic infertile granite (n = 93)*		
Age (Ma)	2832–2658			2932–2660			2676–2626			3010			2703–2701			170–4			430 – 0.6		
Trace element	min	med	max	min	med	max	min	med	max	min	med	max	min	med	max	min	med	max	min	med	max
Ti	2.30	6.15	26.60	1.60	7.70	18.10	4.00	10.85	19.30	2.80	4.80	10.30	1.86	5.80	34.00	0.30	3.80	37.00	0.50	3.80	20.00
Y	343	980	3530	63	520	1620	203	594	1615	282	557	2077	266	632	1850	126	577	5830	581	3434	20 290
Nb	0.36	1.39	6.24	0.36	0.91	3.29	0.60	1.66	3.52	0.43	0.85	2.47	0.35	0.69	1.31	0.18	1.78	59.20	0.83	6.14	570.60
Mo	0.26	0.66	1.61	0.27	1.46	3.59	0.10	0.50	1.67	0.65	1.10	1.41	0.70	1.08	1.95	0.08	0.80	9.40	0.06	0.62	1.15
La	0.01	0.13	0.93	0.01	0.16	0.89	0.01	0.09	0.99	0.01	0.13	0.89	0.00	0.05	0.94	0.00	0.01	0.99	0.00	0.03	0.89
Ce	2.58	9.34	41.00	2.76	11.48	34.50	4.04	8.98	36.10	2.63	7.70	23.20	3.22	8.02	39.30	1.88	22.00	154.00	0.83	15.53	216.90
Pr	0.010	0.149	1.086	0.010	0.075	0.472	0.020	0.088	0.720	0.020	0.137	1.030	0.017	0.099	1.190	0.001	0.050	1.530	0.013	0.129	0.923
Nd	0.58	2.22	10.92	0.16	1.05	4.35	0.29	1.35	6.13	0.30	1.38	7.10	0.29	1.49	11.80	0.03	0.72	23.30	0.25	2.20	13.90
Sm	1.26	3.74	13.50	0.38	1.97	6.88	1.05	2.57	10.72	0.75	1.82	9.03	0.74	2.63	15.30	0.09	1.48	34.90	1.39	6.03	31.40
Eu	0.22	0.74	3.43	0.11	0.42	2.67	0.14	0.48	3.20	0.22	0.67	2.92	0.24	0.95	5.83	0.07	0.75	12.09	0.001	0.20	3.86
Gd	7.20	20.30	79.00	2.01	11.05	42.00	5.63	15.20	43.20	4.61	11.10	47.30	4.54	13.24	54.80	1.31	9.08	137.00	12.00	37.30	205.10
Tb	2.51	6.53	26.10	0.65	3.65	12.86	1.76	4.80	13.47	1.61	3.51	14.09	1.65	4.33	16.50	0.49	3.07	39.20	4.29	14.50	80.50
Dy	30.90	80.50	316.00	6.90	44.85	155.70	19.60	54.30	149.90	20.10	46.50	179.40	19.70	52.05	180.00	7.11	40.60	433.00	51.80	208.30	1035.00
Ho	11.08	31.40	110.30	1.95	17.28	56.20	6.75	19.97	53.50	9.00	17.37	66.10	8.05	20.31	63.80	3.30	16.91	161.30	19.10	83.20	381.20
Er	53.40	157.10	507.00	7.84	84.80	257.30	29.00	88.60	239.00	44.20	88.50	319.00	41.20	93.50	265.00	20.75	93.00	747.00	92.30	394.00	1765.00
Tm	10.53	31.22	96.70	1.37	17.92	50.40	5.65	18.08	47.60	9.67	18.92	64.50	9.82	20.64	51.60	5.30	22.26	148.00	18.24	79.20	341.70
Yb	96	273	814	11	166	452	48	163	425	99	181	570	102	202	449	67	233	1334	155	703	2911
Lu	19.4	58.9	155.6	2.0	34.8	87.0	9.5	33.3	84.1	22.4	39.8	116.0	24.0	45.6	94.2	17.2	57.1	277.7	30.8	137.4	522.0
Hf	6960	8350	10 750	7110	8655	11 270	7270	8650	10 050	7560	9170	12 600	7500	9970	12 060	6016	9062	13 350	6394	10 540	12 560
Ta	0.17	0.53	1.54	0.09	0.34	1.13	0.20	0.59	1.30	0.09	0.30	0.64	0.14	0.32	0.57	0.03	0.50	9.34	0.49	1.85	80.50
Pb	97.3	272.0	2409.0	61.4	190.7	1487.0	65.6	184.1	1029.0	149.2	481.2	1430.0	155.4	496.0	1091.0	0.0	0.8	16.4	0.0	1.0	24.3
Th	15	80	403	11	50	367	21	46	338	26	100	594	38	111	567	4	266	6400	34	159	9850
U	43	109	1020	29	85	634	32	81	452	62	202	586	76	243	519	12	439	4616	72	394	15 710
Eu/Eu*	0.14	0.27	0.53	0.14	0.31	0.72	0.07	0.23	0.65	0.25	0.47	0.67	0.22	0.49	0.80	0.227	0.57	1.46	0.0001	0.06	0.31
Ce/Ce*	3.8	16.6	177.4	4.1	45.3	946.4	2.5	36.5	252.4	3.5	28.2	196.3	3.0	21.6	100.5	6.6	125.2	11 021.0	2.3	41.7	356.9
Yb/Gd	7.0	13.0	25.4	5.3	14.4	32.1	3.5	10.4	20.4	10.3	16.2	26.8	6.6	15.9	25.8	4.2	25.0	93.7	5.3	14.2	45.9
Th/U	0.22	0.55	1.38	0.15	0.61	0.91	0.38	0.58	2.54	0.30	0.51	1.01	0.23	0.44	1.24	0.16	0.59	3.76	0.11	0.53	1.18
T (°C)	651	734	889	624	755	844	696	789	851	667	712	784	635	729	920	517	692	931	547	692	855

NOTES: Eu/Eu* = $Eu_N/(Sm_N \times Gd_N)0.5$, where $_N$ denotes chondrite-normalized values (Sun and McDonough, 1989); Ce/Ce*=$Ce_N/(Nd_N{}^*Nd_N/Sm_N)$ proposed by Loader et al. (2017); Phanerozoic fertile and infertile granitic rock data from Lu et al. (2016)

Table 2. Partition coefficient (K_d) values used in the Rayleigh fractionation model. Italicized values were interpolated or extrapolated from neighbouring partition coefficients by Loader et al. (2017). The grey column is the Boddington diorite sample (BODD-2) whole-rock value used as the starting composition

Mineral	*Titanite*	*Plagioclase*	*Zircon*	*Apatite*	*Amphibole*	*Garnet*	*BODD-2 diorite (ppm, whole rock)*
Rock	*Rhyolite*	*Basaltic andesite*	*Dacite*	*Dacite*	*Tonalite*	*Unknown*	
La	113	0.18	0.00046	36	0.37	0.0109	27.4
Ce	223	0.14	0.36	48	0.73	0.0567	55.6
Pr	***431***	0.13	0.0172	64	–	0.2425	6.2
Nd	639	0.12	0.077	77	1.2	0.8519	22.6
Pm	785	***0.1***	***0.2***	–	–	–	–
Sm	930	0.08	0.8	93	2.01	4.83	3.8
Eu	661	0.79	1.22	55	1.33	8.46	0.7
Gd	855	0.07	8	127	2.3	13.21	2.9
Tb	***895***	0.06	20.7	102	–	18.37	0.3
Dy	935	0.03	45.9	76	2.68	22.76	1.6
Ho	***786***	***0.03***	80	62	–	25.03	0.3
Er	636	0.02	136	57	2.47	25.05	0.9
Tm	***515***	***0.02***	197	53	–	23.33	–
Yb	393	0.01	277	48	2.1	20.64	0.8
Lu	300	0.01	325	33	1.7	17.67	0.1
Pressure (Mpa)	~200	0.1	unknown	unknown	1000	unknown	NA
Temp. (°C)	700–760	1100	unknown	unknown	800	850	NA

Table 3. Results of the amphibole crystallization model, with REE concentrations of model melt compositions and the zircon composition in equilibrium with that melt. The melt starting composition for all models is the BODD-2 whole-rock composition, unless otherwise specified. Abbreviation: F, melt fraction remaining

Amphibole fractionation (%)	*0*	*10*	*20*	*30*	*40*	*50*	*60*	*70*	*80*	*90*	*99*
F	*1*	*0.9*	*0.8*	*0.7*	*0.6*	*0.5*	*0.4*	*0.3*	*0.2*	*0.1*	*0.01*
Model melt compositions											
La	27.40	29.28	31.54	34.30	37.80	42.40	48.80	58.50	75.53	116.88	498.60
Ce	55.60	57.20	59.05	61.22	63.82	67.04	71.21	76.96	85.86	103.53	192.79
Pr	6.20	6.89	7.75	8.86	10.33	12.40	15.50	20.67	31.00	62.00	620.00
Nd	22.60	22.13	21.61	21.04	20.41	19.67	18.82	17.76	16.38	14.26	9.00
Sm	3.80	3.42	3.03	2.65	2.27	1.89	1.51	1.13	0.75	0.37	0.04
Eu	0.70	0.68	0.65	0.62	0.59	0.56	0.52	0.47	0.41	0.33	0.15
Gd	2.90	2.53	2.17	1.82	1.49	1.18	0.88	0.61	0.36	0.15	0.01
Tb	0.30	0.33	0.38	0.43	0.50	0.60	0.75	1.00	1.50	3.00	30.00
Dy	1.60	1.34	1.10	0.88	0.68	0.50	0.34	0.21	0.11	0.03	0.00
Ho	0.30	0.33	0.38	0.43	0.50	0.60	0.75	1.00	1.50	3.00	30.00
Er	0.90	0.77	0.65	0.53	0.42	0.32	0.23	0.15	0.08	0.03	0.00
Yb	0.80	0.71	0.63	0.54	0.46	0.37	0.29	0.21	0.14	0.06	0.01
Lu	0.10	0.09	0.09	0.08	0.07	0.06	0.05	0.04	0.03	0.02	0.00
Yb/Gd (melt)	0.28	0.28	0.29	0.30	0.31	0.32	0.33	0.35	0.38	0.44	0.69
Eu/Eu* (melt)	0.64	0.70	0.77	0.87	0.98	1.14	1.37	1.74	2.43	4.31	28.80
Zircon in equilibrium with model melt compositions											
La	0.013	0.013	0.015	0.016	0.017	0.020	0.022	0.027	0.035	0.054	0.229
Ce	20.02	20.59	21.26	22.04	22.98	24.14	25.63	27.70	30.91	37.27	69.40
Pr	0.107	0.118	0.133	0.152	0.178	0.213	0.267	0.355	0.533	1.066	10.664
Nd	1.74	1.70	1.66	1.62	1.57	1.51	1.45	1.37	1.26	1.10	0.69
Sm	3.04	2.73	2.43	2.12	1.81	1.51	1.20	0.90	0.60	0.30	0.03
Eu	0.85	0.82	0.79	0.76	0.72	0.68	0.63	0.57	0.50	0.40	0.19
Gd	23.20	20.23	17.36	14.59	11.94	9.42	7.05	4.85	2.86	1.16	0.06
Tb	6.21	6.90	7.76	8.87	10.35	12.42	15.53	20.70	31.05	62.10	621.00
Dy	73.44	61.53	50.48	40.34	31.13	22.92	15.75	9.72	4.92	1.53	0.03
Ho	24	27	30	34	40	48	60	80	120	240	2400
Er	122.40	104.84	88.17	72.46	57.76	44.18	31.83	20.85	11.49	4.15	0.14
Yb	221.60	197.35	173.37	149.68	126.34	103.38	80.88	58.94	37.73	17.60	1.40
Lu	32.50	30.19	27.80	25.32	22.73	20.01	17.11	13.99	10.53	6.48	1.29
Yb/Gd (zircon)	9.55	9.76	9.99	10.26	10.58	10.97	11.47	12.15	13.18	15.14	23.99
Eu/Eu* (zircon)	0.31	0.34	0.37	0.42	0.47	0.55	0.66	0.84	1.17	2.08	13.89

Table 4. Results of the apatite crystallization model, with REE concentrations of model melt compositions and the zircon composition in equilibrium with that melt

Apatite fractionation (%)	*0*	*0.2*	*0.4*	*0.6*	*0.8*	*1*	*1.2*	*1.4*	*1.6*	*1.8*	*2*
F	*1*	*0.998*	*0.996*	*0.994*	*0.992*	*0.99*	*0.988*	*0.986*	*0.984*	*0.982*	*0.98*
Model melt compositions											
La	27.40	25.55	23.81	22.20	20.69	19.27	17.96	16.73	15.58	14.51	13.51
Ce	55.60	50.61	46.05	41.90	38.12	34.67	31.52	28.66	26.05	23.68	21.51
Pr	6.20	5.47	4.82	4.24	3.74	3.29	2.90	2.55	2.24	1.97	1.74
Nd	22.60	19.41	16.67	14.30	12.27	10.53	9.03	7.74	6.63	5.68	4.87
Sm	3.80	3.16	2.63	2.18	1.81	1.51	1.25	1.04	0.86	0.71	0.59
Eu	0.70	0.63	0.56	0.51	0.45	0.41	0.36	0.33	0.29	0.26	0.24
Gd	2.90	2.25	1.75	1.36	1.05	0.82	0.63	0.49	0.38	0.29	0.23
Tb	0.30	0.25	0.20	0.16	0.13	0.11	0.09	0.07	0.06	0.05	0.04
Dy	1.60	1.38	1.18	1.02	0.88	0.75	0.65	0.56	0.48	0.41	0.35
Ho	0.30	0.27	0.23	0.21	0.18	0.16	0.14	0.13	0.11	0.10	0.09
Er	0.90	0.80	0.72	0.64	0.57	0.51	0.46	0.41	0.36	0.33	0.29
Yb	0.80	0.73	0.66	0.60	0.55	0.50	0.45	0.41	0.37	0.34	0.31
Lu	0.10	0.09	0.09	0.08	0.08	0.07	0.07	0.06	0.06	0.06	0.05
Yb/Gd (melt)	0.28	0.32	0.38	0.44	0.52	0.61	0.72	0.84	0.99	1.16	1.36
Eu/Eu* (melt)	0.64	0.72	0.80	0.90	1.00	1.12	1.25	1.40	1.57	1.75	1.96
Zircon in equilibrium with model melt compositions											
La	0.013	0.012	0.011	0.010	0.010	0.009	0.008	0.008	0.007	0.007	0.006
Ce	20.02	18.22	16.58	15.08	13.72	12.48	11.35	10.32	9.38	8.52	7.74
Pr	0.107	0.094	0.083	0.073	0.064	0.057	0.050	0.044	0.039	0.034	0.030
Nd	1.74	1.49	1.28	1.10	0.95	0.81	0.70	0.60	0.51	0.44	0.37
Sm	3.04	2.53	2.10	1.75	1.45	1.21	1.00	0.83	0.69	0.57	0.47
Eu	0.85	0.77	0.69	0.62	0.55	0.50	0.44	0.40	0.36	0.32	0.29
Gd	23.20	18.03	14.00	10.87	8.43	6.54	5.07	3.93	3.04	2.35	1.82
Tb	6.21	5.07	4.14	3.38	2.76	2.25	1.83	1.50	1.22	0.99	0.81
Dy	73.44	63.20	54.37	46.76	40.21	34.56	29.70	25.51	21.91	18.81	16.14
Ho	24.00	21.24	18.79	16.63	14.70	13.00	11.49	10.16	8.97	7.93	7.00
Er	122.40	109.42	97.79	87.38	78.06	69.72	62.25	55.58	49.60	44.26	39.49
Yb	221.60	201.70	183.55	167.01	151.92	138.17	125.65	114.23	103.83	94.36	85.74
Lu	32.50	30.48	28.59	26.81	25.13	23.56	22.09	20.70	19.40	18.17	17.03
Yb/Gd (zircon)	9.55	11.19	13.11	15.37	18.02	21.13	24.79	29.09	34.16	40.11	47.12
Eu/Eu* (zircon)	0.31	0.35	0.39	0.43	0.48	0.54	0.60	0.68	0.75	0.84	0.94

Table 5. Results of the titanite crystallization model, with REE concentrations of model melt compositions and the zircon composition in equilibrium with that melt

Titanite fractionation (%)	*0*	*0.05*	*0.1*	*0.15*	*0.2*	*0.25*	*0.3*	*0.35*	*0.4*	*0.45*	*0.5*
F	*1*	*0.9995*	*0.999*	*0.9985*	*0.998*	*0.9975*	*0.997*	*0.9965*	*0.996*	*0.9955*	*0.995*
Model melt compositions											
La	27.40	25.91	24.50	23.16	21.90	20.70	19.57	18.50	17.49	16.53	15.63
Ce	55.60	49.76	44.53	39.84	35.65	31.90	28.54	25.53	22.84	20.43	18.27
Pr	6.20	5.00	4.03	3.25	2.62	2.11	1.70	1.37	1.11	0.89	0.72
Nd	22.60	16.43	11.94	8.67	6.30	4.58	3.32	2.41	1.75	1.27	0.92
Sm	3.80	2.39	1.50	0.94	0.59	0.37	0.23	0.15	0.09	0.06	0.04
Eu	0.70	0.50	0.36	0.26	0.19	0.13	0.10	0.07	0.05	0.04	0.03
Gd	2.90	1.89	1.23	0.80	0.52	0.34	0.22	0.15	0.09	0.06	0.04
Tb	0.30	0.19	0.12	0.08	0.05	0.03	0.02	0.01	0.01	0.01	0.00
Dy	1.60	1.00	0.63	0.39	0.25	0.15	0.10	0.06	0.04	0.02	0.01
Ho	0.30	0.20	0.14	0.09	0.06	0.04	0.03	0.02	0.01	0.01	0.01
Er	0.90	0.66	0.48	0.35	0.25	0.18	0.13	0.10	0.07	0.05	0.04
Yb	0.80	0.66	0.54	0.44	0.36	0.30	0.25	0.20	0.17	0.14	0.11
Lu	0.10	0.09	0.07	0.06	0.05	0.05	0.04	0.04	0.03	0.03	0.02
Yb/Gd (melt)	0.28	0.35	0.44	0.55	0.70	0.88	1.11	1.39	1.76	2.22	2.80
Eu/Eu* (melt)	0.64	0.72	0.81	0.91	1.02	1.15	1.29	1.45	1.63	1.83	2.06
Zircon in equilibrium with model melt compositions											
La	0.013	0.012	0.011	0.011	0.010	0.010	0.009	0.009	0.008	0.008	0.007
Ce	20.02	17.91	16.03	14.34	12.83	11.48	10.27	9.19	8.22	7.35	6.58
Pr	0.107	0.086	0.069	0.056	0.045	0.036	0.029	0.024	0.019	0.015	0.012
Nd	1.74	1.26	0.92	0.67	0.49	0.35	0.26	0.19	0.13	0.10	0.07
Sm	3.04	1.91	1.20	0.75	0.47	0.30	0.19	0.12	0.07	0.05	0.03
Eu	0.85	0.61	0.44	0.32	0.23	0.16	0.12	0.08	0.06	0.04	0.03
Gd	23.20	15.14	9.87	6.44	4.20	2.74	1.78	1.16	0.76	0.49	0.32
Tb	6.21	3.97	2.54	1.62	1.04	0.66	0.42	0.27	0.17	0.11	0.07
Dy	73.44	46.03	28.85	18.07	11.32	7.09	4.44	2.78	1.74	1.09	0.68
Ho	24.00	16.21	10.94	7.39	4.99	3.36	2.27	1.53	1.03	0.70	0.47
Er	122.40	89.10	64.84	47.19	34.33	24.97	18.16	13.21	9.60	6.98	5.08
Yb	221.60	182.15	149.71	123.03	101.10	83.07	68.25	56.06	46.05	37.82	31.06
Lu	32.50	27.99	24.10	20.75	17.86	15.38	13.24	11.39	9.80	8.44	7.26
Yb/Gd (zircon)	9.55	12.03	15.16	19.11	24.09	30.36	38.28	48.26	60.85	76.74	96.79
Eu/Eu* (zircon)	0.31	0.35	0.39	0.44	0.49	0.55	0.62	0.70	0.79	0.88	0.99

Table 6. Results of the plagioclase crystallization model, with REE concentrations of model melt compositions and the zircon composition in equilibrium with that melt

Plagioclase fractionation (%)	*0*	*10*	*20*	*30*	*40*	*50*	*60*	*70*	*80*	*90*	*99*
F	*1*	*0.9*	*0.8*	*0.7*	*0.6*	*0.5*	*0.4*	*0.3*	*0.2*	*0.1*	*0.01*
Model melt compositions											
La	27.40	29.87	32.90	36.71	41.65	48.37	58.08	73.54	102.54	181.03	1196.05
Ce	55.60	60.87	67.36	75.56	86.27	100.92	122.27	156.59	221.92	402.79	2917.93
Pr	6.20	6.80	7.53	8.46	9.67	11.33	13.76	17.67	25.15	45.96	340.72
Nd	22.60	24.80	27.50	30.93	35.43	41.59	50.62	65.20	93.15	171.44	1300.49
Sm	3.80	4.19	4.67	5.28	6.08	7.19	8.83	11.50	16.70	31.61	262.90
Eu	0.70	0.72	0.73	0.75	0.78	0.81	0.85	0.90	0.98	1.14	1.84
Gd	2.90	3.20	3.57	4.04	4.66	5.53	6.80	8.89	12.96	24.68	210.09
Tb	0.30	0.33	0.37	0.42	0.48	0.58	0.71	0.93	1.36	2.61	22.76
Dy	1.60	1.77	1.99	2.26	2.63	3.13	3.89	5.14	7.62	14.93	139.35
Ho	0.30	0.33	0.37	0.42	0.49	0.59	0.73	0.96	1.43	2.80	26.13
Er	0.90	1.00	1.12	1.28	1.48	1.78	2.21	2.93	4.36	8.59	82.08
Yb	0.80	0.89	1.00	1.14	1.33	1.59	1.98	2.63	3.94	7.82	76.40
Lu	0.10	0.11	0.12	0.14	0.17	0.20	0.25	0.33	0.49	0.98	9.55
Yb/Gd (melt)	0.28	0.28	0.28	0.28	0.28	0.29	0.29	0.30	0.30	0.32	0.36
Eu/Eu* (melt)	0.64	0.60	0.55	0.50	0.45	0.39	0.33	0.27	0.20	0.12	0.02
Zircon in equilibrium with model melt compositions											
La	0.013	0.014	0.015	0.017	0.019	0.022	0.027	0.034	0.047	0.083	0.550
Ce	20.02	21.91	24.25	27.20	31.06	36.33	44.02	56.37	79.89	145.00	1050.45
Pr	0.107	0.117	0.129	0.145	0.166	0.195	0.237	0.304	0.433	0.791	5.860
Nd	1.74	1.91	2.12	2.38	2.73	3.20	3.90	5.02	7.17	13.20	100.14
Sm	3.04	3.35	3.73	4.22	4.86	5.75	7.06	9.20	13.36	25.29	210.32
Eu	0.85	0.87	0.89	0.92	0.95	0.99	1.04	1.10	1.20	1.39	2.25
Gd	23.20	25.59	28.55	32.33	37.31	44.20	54.40	71.08	103.64	197.46	1680.69
Tb	6.21	6.86	7.66	8.68	10.04	11.91	14.69	19.26	28.19	54.09	471.08
Dy	73	81	91	104	121	144	179	236	350	685	6396
Ho	24	27	30	34	39	47	58	77	114	224	2090
Er	122	136	152	174	202	241	300	398	593	1169	11 163
Yb	222	246	276	315	367	440	549	730	1090	2166	21 163
Lu	33	36	41	46	54	65	81	107	160	318	3104
Yb/Gd (zircon)	9.55	9.61	9.68	9.76	9.85	9.96	10.09	10.27	10.52	10.97	12.59
Eu/Eu* (zircon)	0.31	0.29	0.27	0.24	0.22	0.19	0.16	0.13	0.10	0.06	0.01

Table 7. Results of the zircon crystallization model, with REE concentrations of model melt compositions and the zircon composition in equilibrium with that melt

Zircon fractionation (%)	*0*	*0.2*	*0.4*	*0.6*	*0.8*	*1*	*1.2*	*1.4*	*1.6*	*1.8*	*2*
F	*1*	*0.998*	*0.996*	*0.994*	*0.992*	*0.99*	*0.988*	*0.986*	*0.984*	*0.982*	*0.98*
Model melt compositions											
La	27.40	27.45	27.51	27.57	27.62	27.68	27.73	27.79	27.85	27.90	27.96
Ce	55.60	55.67	55.74	55.81	55.89	55.96	56.03	56.10	56.18	56.25	56.32
Pr	6.20	6.21	6.22	6.24	6.25	6.26	6.27	6.29	6.30	6.31	6.32
Nd	22.60	22.64	22.68	22.73	22.77	22.81	22.85	22.90	22.94	22.98	23.03
Sm	3.80	3.80	3.80	3.80	3.81	3.81	3.81	3.81	3.81	3.81	3.82
Eu	0.70	0.70	0.70	0.70	0.70	0.70	0.70	0.70	0.70	0.70	0.70
Gd	2.90	2.86	2.82	2.78	2.74	2.70	2.66	2.63	2.59	2.55	2.52
Tb	0.30	0.29	0.28	0.27	0.26	0.25	0.24	0.23	0.22	0.21	0.20
Dy	1.60	1.46	1.34	1.22	1.12	1.02	0.93	0.85	0.78	0.71	0.65
Ho	0.30	0.26	0.22	0.19	0.16	0.14	0.12	0.10	0.08	0.07	0.06
Er	0.90	0.69	0.52	0.40	0.30	0.23	0.18	0.13	0.10	0.08	0.06
Yb	0.80	0.46	0.26	0.15	0.09	0.05	0.03	0.02	0.01	0.01	0.00
Lu	0.10	0.05	0.03	0.01	0.01	0.00	0.00	0.00	0.00	0.00	0.00
Yb/Gd (melt)	0.28	0.16	0.09	0.05	0.03	0.02	0.01	0.01	0.00	0.00	0.00
Eu/Eu* (melt)	0.64	0.65	0.65	0.66	0.66	0.67	0.67	0.67	0.68	0.68	0.69
Zircon in equilibrium with model melt compositions											
La	0.013	0.013	0.013	0.013	0.013	0.013	0.013	0.013	0.013	0.013	0.013
Ce	20.02	20.04	20.07	20.09	20.12	20.15	20.17	20.20	20.22	20.25	20.28
Pr	0.107	0.107	0.107	0.107	0.107	0.108	0.108	0.108	0.108	0.109	0.109
Nd	1.74	1.74	1.75	1.75	1.75	1.76	1.76	1.76	1.77	1.77	1.77
Sm	3.04	3.04	3.04	3.04	3.04	3.05	3.05	3.05	3.05	3.05	3.05
Eu	0.85	0.85	0.85	0.85	0.85	0.85	0.85	0.85	0.85	0.85	0.85
Gd	23.20	22.88	22.56	22.24	21.93	21.62	21.32	21.02	20.72	20.43	20.14
Tb	6.21	5.97	5.74	5.52	5.30	5.09	4.90	4.70	4.52	4.34	4.17
Dy	73.44	67.13	61.34	56.05	51.20	46.77	42.71	38.99	35.60	32.49	29.65
Ho	24.00	20.49	17.49	14.92	12.72	10.85	9.25	7.88	6.71	5.72	4.86
Er	122.40	93.41	71.25	54.32	41.39	31.52	23.99	18.25	13.87	10.54	8.00
Yb	221.60	127.53	73.31	42.09	24.14	13.83	7.92	4.52	2.58	1.47	0.84
Lu	32.50	16.99	8.87	4.62	2.41	1.25	0.65	0.34	0.17	0.09	0.05
Yb/Gd (zircon)	9.55	5.57	3.25	1.89	1.10	0.64	0.37	0.22	0.12	0.07	0.04
Eu/Eu* (zircon)	0.31	0.31	0.31	0.32	0.32	0.32	0.32	0.33	0.33	0.33	0.33

Table 8. Results of the garnet crystallization model, with REE concentrations of model melt compositions and the zircon composition in equilibrium with that melt

Garnet fractionation (%)	*0*	*5*	*10*	*15*	*20*	*25*	*30*	*35*	*40*	*45*	*50*
F	*1*	*0.95*	*0.9*	*0.85*	*0.8*	*0.75*	*0.7*	*0.65*	*0.6*	*0.55*	*0.5*
Model melt compositions											
La	27.40	28.83	30.41	32.18	34.17	36.42	38.99	41.96	45.41	49.50	54.39
Ce	55.60	58.36	61.41	64.81	68.63	72.93	77.84	83.48	90.02	97.72	106.92
Pr	6.20	6.45	6.72	7.01	7.34	7.71	8.12	8.59	9.13	9.75	10.48
Nd	22.60	22.77	22.96	23.15	23.36	23.58	23.83	24.09	24.38	24.69	25.04
Sm	3.80	3.12	2.54	2.04	1.62	1.26	0.97	0.73	0.54	0.38	0.27
Eu	0.70	0.48	0.32	0.21	0.13	0.08	0.05	0.03	0.02	0.01	0.00
Gd	2.90	1.55	0.80	0.40	0.19	0.09	0.04	0.02	0.01	0.00	0.00
Tb	0.30	0.12	0.05	0.02	0.01	0.00	0.00	0.00	0.00	0.00	0.00
Dy	1.60	0.52	0.16	0.05	0.01	0.00	0.00	0.00	0.00	0.00	0.00
Ho	0.30	0.09	0.02	0.01	0.00	0.00	0.00	0.00	0.00	0.00	0.00
Er	0.90	0.26	0.07	0.02	0.00	0.00	0.00	0.00	0.00	0.00	0.00
Yb	0.80	0.29	0.10	0.03	0.01	0.00	0.00	0.00	0.00	0.00	0.00
Lu	0.10	0.04	0.02	0.01	0.00	0.00	0.00	0.00	0.00	0.00	0.00
Yb/Gd (melt)	0.28	0.19	0.13	0.08	0.05	0.03	0.02	0.01	0.01	0.00	0.00
Eu/Eu* (melt)	0.64	0.66	0.68	0.71	0.73	0.76	0.79	0.82	0.86	0.90	0.95
Zircon in equilibrium with model melt compositions											
La	0.013	0.013	0.014	0.015	0.016	0.017	0.018	0.019	0.021	0.023	0.025
Ce	20.02	21.01	22.11	23.33	24.71	26.26	28.02	30.05	32.41	35.18	38.49
Pr	0.107	0.111	0.115	0.121	0.126	0.133	0.140	0.148	0.157	0.168	0.180
Nd	1.74	1.75	1.77	1.78	1.80	1.82	1.83	1.85	1.88	1.90	1.93
Sm	3.04	2.50	2.03	1.63	1.29	1.01	0.78	0.58	0.43	0.31	0.21
Eu	0.85	0.58	0.39	0.25	0.16	0.10	0.06	0.03	0.02	0.01	0.00
Gd	23.20	12.40	6.41	3.19	1.52	0.69	0.30	0.12	0.05	0.02	0.00
Tb	6.21	2.55	1.00	0.37	0.13	0.04	0.01	0.00350	0.00087	0.00019	0.00004
Dy	73.44	24.06	7.42	2.14	0.57	0.14	0.03	0.00625	0.00109	0.00016	0.00002
Ho	24.00	7.00	1.91	0.48	0.11	0.02	0.005	0.0008	0.00011	0.00001	0.000001
Er	122.40	35.65	9.71	2.46	0.57	0.12	0.02	0.00388	0.00057	0.00007	0.00001
Yb	221.60	80.91	27.98	9.10	2.77	0.78	0.20	0.04686	0.00973	0.00176	0.00027
Lu	32.50	13.82	5.61	2.16	0.79	0.27	0.08	0.02470	0.00650	0.00152	0.00031
Yb/Gd (zircon)	9.55	6.52	4.36	2.85	1.82	1.13	0.67	0.39	0.21	0.11	0.06
Eu/Eu* (zircon)	0.31	0.32	0.33	0.34	0.35	0.36	0.38	0.40	0.41	0.43	0.46

Table 9. Results of the amphibole:apatite (99.8 : 0.2) crystallization model, with REE concentrations of model melt compositions and the zircon composition in equilibrium with that melt. The column in bold (40% crystallization) was the hypothetical melt used as starting composition for one plagioclase:apatite (98.7 : 1.3) fractionation (Table 10)

Fractionation (%)	*0*	*5*	*10*	*15*	*20*	*25*	*30*	*35*	*40*	*45*	*50*
F	*1*	*0.95*	*0.9*	*0.85*	*0.8*	*0.75*	*0.7*	*0.65*	*0.6*	*0.55*	*0.5*
Model melt compositions											
La	27.40	28.20	29.06	30.00	31.04	32.18	33.44	34.86	**36.45**	38.27	40.36
Ce	55.60	56.10	56.64	57.21	57.82	58.48	59.19	59.97	**60.81**	61.75	62.79
Pr	6.20	6.48	6.80	7.14	7.53	7.97	8.46	9.03	**9.68**	10.44	11.35
Nd	22.60	22.20	21.78	21.34	20.89	20.43	19.94	19.42	**18.88**	18.32	17.71
Sm	3.80	3.57	3.35	3.13	2.91	2.70	2.48	2.27	**2.07**	1.86	1.66
Eu	0.70	0.68	0.67	0.65	0.63	0.62	0.60	0.58	**0.56**	0.54	0.52
Gd	2.90	2.68	2.46	2.25	2.05	1.86	1.67	1.49	**1.31**	1.15	0.99
Tb	0.30	0.31	0.33	0.34	0.36	0.38	0.40	0.42	**0.45**	0.48	0.52
Dy	1.60	1.46	1.32	1.19	1.06	0.95	0.83	0.73	**0.63**	0.54	0.45
Ho	0.30	0.31	0.33	0.35	0.36	0.39	0.41	0.44	**0.47**	0.51	0.55
Er	0.90	0.83	0.76	0.70	0.63	0.57	0.51	0.46	**0.40**	0.35	0.30
Yb	0.80	0.75	0.71	0.66	0.61	0.57	0.52	0.48	**0.44**	0.39	0.35
Lu	0.10	0.10	0.09	0.09	0.08	0.08	0.08	0.07	**0.07**	0.06	0.06
Yb/Gd (melt)	0.28	0.28	0.29	0.29	0.30	0.31	0.31	0.32	**0.33**	0.34	0.35
Eu/Eu* (melt)	0.64	0.68	0.71	0.75	0.79	0.84	0.90	0.96	**1.04**	1.13	1.23
Zircon in equilibrium with model melt compositions											
La	0.013	0.013	0.013	0.014	0.014	0.015	0.015	0.016	**0.017**	0.018	0.019
Ce	20.02	20.20	20.39	20.59	20.82	21.05	21.31	21.59	**21.89**	22.23	22.60
Pr	0.107	0.112	0.117	0.123	0.130	0.137	0.146	0.155	**0.166**	0.180	0.195
Nd	1.74	1.71	1.68	1.64	1.61	1.57	1.54	1.50	**1.45**	1.41	1.36
Sm	3.04	2.86	2.68	2.50	2.33	2.16	1.99	1.82	**1.65**	1.49	1.33
Eu	0.85	0.84	0.82	0.80	0.77	0.75	0.73	0.71	**0.68**	0.66	0.63
Gd	23.20	21.43	19.71	18.04	16.42	14.86	13.35	11.90	**10.51**	9.19	7.93
Tb	6.21	6.47	6.75	7.07	7.42	7.81	8.25	8.75	**9.33**	9.99	10.78
Dy	73.44	66.87	60.58	54.58	48.86	43.42	38.28	33.43	**28.89**	24.64	20.70
Ho	24.00	25.10	26.32	27.67	29.18	30.88	32.80	35.00	**37.54**	40.52	44.05
Er	122.40	112.88	103.64	94.70	86.05	77.71	69.69	62.00	**54.63**	47.62	40.97
Yb	221.60	208.46	195.45	182.58	169.85	157.28	144.86	132.62	**120.55**	108.68	97.01
Lu	32.50	31.25	29.99	28.71	27.41	26.10	24.76	23.40	**22.01**	20.60	19.16
Yb/Gd (zircon)	9.55	9.73	9.92	10.12	10.35	10.59	10.85	11.14	**11.47**	11.83	12.24
Eu/Eu* (zircon)	0.31	0.33	0.34	0.36	0.38	0.41	0.43	0.46	**0.50**	0.54	0.59

Table 10. Results of the plagioclase:apatite (98.7 : 1.3) crystallization model, using melt starting composition of the hypothetical melt after 40% crystallization of the amphibole:apatite (99.8 : 0.2) fractionation in Table 9

Fractionation (%)	*0*	*10*	*20*	*30*	*40*	*50*	*60*	*70*	*80*	*90*	*99*
F	*1*	*0.9*	*0.8*	*0.7*	*0.6*	*0.5*	*0.4*	*0.3*	*0.2*	*0.1*	*0.01*
Model melt compositions											
La	**36.45**	37.84	39.45	41.36	43.68	46.60	50.43	55.84	64.47	82.42	186.37
Ce	**60.81**	62.36	64.13	66.20	68.67	71.71	75.62	80.98	89.17	105.15	181.82
Pr	**9.68**	9.72	9.77	9.82	9.88	9.95	10.04	10.15	10.32	10.61	11.62
Nd	**18.88**	18.65	18.39	18.10	17.77	17.38	16.93	16.36	15.58	14.34	10.89
Sm	**2.07**	2.01	1.94	1.87	1.78	1.69	1.59	1.46	1.30	1.07	0.55
Eu	**0.56**	0.53	0.50	0.47	0.43	0.40	0.36	0.31	0.25	0.18	0.06
Gd	**1.31**	1.22	1.12	1.02	0.91	0.80	0.68	0.55	0.41	0.25	0.05
Tb	**0.45**	0.43	0.41	0.39	0.37	0.34	0.32	0.28	0.24	0.19	0.08
Dy	**0.63**	0.63	0.63	0.63	0.62	0.62	0.62	0.62	0.61	0.60	0.58
Ho	**0.47**	0.48	0.49	0.50	0.51	0.53	0.55	0.57	0.61	0.69	1.00
Er	**0.40**	0.41	0.42	0.44	0.45	0.47	0.50	0.54	0.59	0.70	1.21
Yb	**0.44**	0.45	0.47	0.50	0.52	0.56	0.61	0.68	0.78	1.01	2.35
Lu	**0.07**	0.07	0.08	0.08	0.09	0.10	0.11	0.13	0.17	0.25	0.90
Yb/Gd (melt)	**0.33**	0.37	0.42	0.49	0.58	0.70	0.90	1.22	1.90	4.04	49.26
Eu/Eu* (melt)	**1.04**	1.04	1.04	1.04	1.04	1.05	1.05	1.05	1.05	1.06	1.08
Zircon in equilibrium with model melt compositions											
La	**0.017**	0.017	0.018	0.019	0.020	0.021	0.023	0.026	0.030	0.038	0.086
Ce	**21.89**	22.45	23.09	23.83	24.72	25.82	27.22	29.15	32.10	37.85	65.46
Pr	**0.166**	0.167	0.168	0.169	0.170	0.171	0.173	0.175	0.177	0.182	0.200
Nd	**1.45**	1.44	1.42	1.39	1.37	1.34	1.30	1.26	1.20	1.10	0.84
Sm	**1.65**	1.60	1.55	1.49	1.43	1.35	1.27	1.17	1.04	0.85	0.44
Eu	**0.68**	0.65	0.61	0.57	0.53	0.48	0.43	0.38	0.31	0.22	0.07
Gd	**10.51**	9.75	8.95	8.13	7.28	6.38	5.44	4.42	3.30	2.00	0.38
Tb	**9.33**	8.95	8.56	8.13	7.66	7.14	6.55	5.86	5.02	3.84	1.58
Dy	**28.89**	28.83	28.77	28.71	28.63	28.54	28.42	28.28	28.08	27.74	26.64
Ho	**37.54**	38.20	38.95	39.81	40.83	42.08	43.65	45.76	48.92	54.82	80.04
Er	**54.63**	56.03	57.63	59.50	61.74	64.49	68.03	72.87	80.30	94.78	164.43
Yb	**120.55**	125.29	130.81	137.37	145.34	155.38	168.60	187.33	217.31	280.09	650.77
Lu	**22.01**	23.35	24.95	26.89	29.32	32.48	36.81	43.26	54.31	80.14	291.72
Yb/Gd (zircon)	**11.47**	12.86	14.61	16.89	19.97	24.34	31.02	42.40	65.86	139.84	1705.51
Eu/Eu* (zircon)	**0.50**	0.50	0.50	0.50	0.50	0.50	0.51	0.51	0.51	0.51	0.52

Table 11. Results of the plagioclase:apatite (98.7 : 1.3) crystallization model using melt starting composition of BODD-2 sample

Fractionation (%)	*0*	*10*	*20*	*30*	*40*	*50*	*60*	*70*	*80*	*90*	*99*
F	*1*	*0.9*	*0.8*	*0.7*	*0.6*	*0.5*	*0.4*	*0.3*	*0.2*	*0.1*	*0.01*
Model melt compositions											
La	27.40	28.44	29.65	31.09	32.84	35.03	37.91	41.98	48.46	61.96	140.10
Ce	55.60	57.01	58.63	60.52	62.78	65.56	69.14	74.03	81.53	96.14	166.23
Pr	6.20	6.23	6.26	6.29	6.33	6.37	6.43	6.50	6.61	6.79	7.44
Nd	22.60	22.32	22.01	21.66	21.26	20.80	20.26	19.57	18.65	17.17	13.04
Sm	3.80	3.69	3.56	3.43	3.28	3.11	2.92	2.69	2.39	1.96	1.01
Eu	0.70	0.66	0.63	0.59	0.54	0.50	0.44	0.39	0.32	0.22	0.07
Gd	2.90	2.69	2.47	2.24	2.01	1.76	1.50	1.22	0.91	0.55	0.11
Tb	0.30	0.29	0.28	0.26	0.25	0.23	0.21	0.19	0.16	0.12	0.05
Dy	1.60	1.60	1.59	1.59	1.59	1.58	1.57	1.57	1.56	1.54	1.48
Ho	0.30	0.31	0.31	0.32	0.33	0.34	0.35	0.37	0.39	0.44	0.64
Er	0.90	0.92	0.95	0.98	1.02	1.06	1.12	1.20	1.32	1.56	2.71
Yb	0.80	0.83	0.87	0.91	0.96	1.03	1.12	1.24	1.44	1.86	4.32
Lu	0.10	0.11	0.11	0.12	0.13	0.15	0.17	0.20	0.25	0.36	1.33
Yb/Gd (melt)	0.28	0.31	0.35	0.41	0.48	0.59	0.75	1.02	1.58	3.36	41.03
Eu/Eu* (melt)	0.64	0.65	0.65	0.65	0.65	0.65	0.65	0.65	0.65	0.66	0.67
Zircon in equilibrium with model melt compositions											
La	0.013	0.013	0.014	0.014	0.015	0.016	0.017	0.019	0.022	0.029	0.064
Ce	20.02	20.52	21.11	21.79	22.60	23.60	24.89	26.65	29.35	34.61	59.84
Pr	0.107	0.107	0.108	0.108	0.109	0.110	0.111	0.112	0.114	0.117	0.128
Nd	1.74	1.72	1.69	1.67	1.64	1.60	1.56	1.51	1.44	1.32	1.00
Sm	3.04	2.95	2.85	2.74	2.62	2.49	2.33	2.15	1.91	1.57	0.81
Eu	0.85	0.81	0.76	0.72	0.66	0.61	0.54	0.47	0.39	0.27	0.09
Gd	23.20	21.50	19.76	17.95	16.06	14.08	11.99	9.75	7.28	4.42	0.84
Tb	6.21	5.96	5.70	5.41	5.10	4.75	4.36	3.91	3.34	2.56	1.05
Dy	73.44	73.30	73.15	72.98	72.78	72.55	72.26	71.90	71.39	70.52	67.72
Ho	24.00	24.42	24.90	25.45	26.10	26.90	27.90	29.25	31.27	35.04	51.17
Er	122.40	125.52	129.11	133.30	138.31	144.48	152.40	163.26	179.89	212.34	368.38
Yb	221.60	230.32	240.46	252.51	267.17	285.62	309.93	344.36	399.47	514.87	1196.27
Lu	32.50	34.48	36.84	39.70	43.29	47.95	54.35	63.87	80.19	118.31	430.67
Yb/Gd (zircon)	9.55	10.71	12.17	14.07	16.64	20.28	25.84	35.32	54.87	116.49	1420.76
Eu/Eu* (zircon)	0.31	0.31	0.31	0.31	0.31	0.31	0.31	0.31	0.32	0.32	0.32

References

Alonso-Perez, R, Müntener, O and Ulmer, P 2009, Igneous garnet and amphibole fractionation in the roots of island arcs: experimental constraints on andesitic liquids: Contributions to Mineralogy and Petrology, v. 157, p. 541–558.

Bachmann, O, Dungan, MA and Bussy, F 2005, Insights into shallow magmatic processes in large silicic magma bodies: the trace element record in the Fish Canyon magma body, Colorado: Contributions to Mineralogy and Petrology, v. 149, p. 338–349.

Ballard, JR, Palin, JM and Campbell, IH 2002, Relative oxidation states of magmas inferred from Ce(IV)/Ce(III) in zircon: Application to porphyry copper deposits of northern Chile: Contributions to Mineralogy and Petrology, v. 144, p. 347–364.

Barley, ME 1982, Porphyry-style mineralization associated with early Archaean calc-alkaline igneous activity, eastern Pilbara, western Australia: Economic Geology, v. 77, p. 1230–1236.

Bell, EA, Boehnke, P and Harrison, TM 2016, Recovering the primary geochemistry of Jack Hills zircons through quantitative estimates of chemical alteration: Geochimica et Cosmochimica Acta, v. 191, p. 187–202.

Blevin, PL 2004, Redox and compositional parameters for interpreting granitoid metallogeny of eastern Australia: implications for gold-rich ore systems: Resource Geology, v. 54, p. 241–252.

Brett, JW 2019, 400 m Bouguer gravity merged grid of Western Australia 2019 version 1: Geological Survey of Western Australia, <www.dmp.wa.gov.au/geophysics>.

Bouvier, A, Ushikubo, T, Kita, NT, Cavosie, AJ, Kozdon, R and Valley, JW 2012, Li isotopes and trace elements as a petrogenetic tracer in zircon: Insights from Archean TTGs and sanukitoids: Contributions to Mineralogy and Petrology, v. 163, p. 745–768.

Burnham, CW, 1979, Magmas and hydrothermal fluids, *in* Geochemistry of hydrothermal ore deposits *edited by* HL Barnes: New York, Wiley, p. 71–136.

Burnham, AD and Berry, AJ 2012, An experimental study of trace element partitioning between zircon and melt as a function of oxygen fugacity: Geochimica et Cosmochimica Acta, v. 95, p. 196–212.

Burnham, AD and Berry, AJ 2014, The effect of oxygen fugacity, melt composition, temperature and pressure on the oxidation state of cerium in silicate melts: Chemical Geology, v. 366, p. 52–60.

Burnham, AD, Berry, AJ, Halse, HR, Schofield, PF, Cibin, G and Mosselmans, JFW 2015, The oxidation state of Eu in silicate melts as a function of oxygen fugacity, composition and temperature: Chemical Geology, v. 411, p. 248–259.

Burnham, AD and Berry, AJ 2017, Formation of Hadean granites by melting of igneous crust: Nature Geoscience, v. 10, p. 457–461.

Chiaradia, M, Ulianov, A, Kouzmanov, K and Beate, B 2012, Why large porphyry Cu deposits like high Sr/Y magmas?: Scientific Reports 2, no. 685, 7p., doi:10.1038/srep00685.

Claiborne, LL, Miller, CF and Wooden, JL 2010, Trace element composition of igneous zircon: a thermal and compositional record of the accumulation and evolution of a large silicic batholith, Spirit Mountain, Nevada: Contributions to Mineralogy and Petrology, v. 160, p. 511–531.

Cooke, DR, Hollings, P and Walshe, JL 2005, Giant porphyry deposits: characteristics, distribution and tectonic controls: Economic Geology, v. 100, p. 801–818.

Dilles, JH, Kent, AJR, Wooden, JL, Tosdal, RM, Koleszar, A, Lee, RG and Farmer, LP 2015, Zircon compositional evidence for sulfur-degassing from ore-forming arc magmas: Economic Geology, v. 110, p. 241–251.

Dunn, T and Sen, C 1994, Mineral/matrix partition coefficients for orthopyroxene, plagioclase, and olivine in basaltic to andesitic systems: a combined analytical and experimental study: Geochimica et Cosmochimica Acta, v. 58, p. 717–733.

Fayol, N and Jebrak, M 2017, Archean sanukitoid gold porphyry deposits: A new understanding and genetic model from the Lac Bachelor gold deposit, Abititi, Canada: Economic Geology, v. 112, p. 1913–1936.

Helt, KM, Williams-Jones, AE, Clark, JR, Wing, BA and Wares, RP 2014, Constraints on the genesis of the Archean oxidized, intrusion-related Canadian Malartic gold deposit, Quebec, Canada: Economic Geology, v. 109, p. 713–735.

Hronsky, JMA, Groves, DI, Loucks, RR and Begg, GC 2012, A unified model for gold mineralization in accretionary orogens and implications for regional-scale exploration targeting methods: Mineralium Deposita, v. 47, p. 339–358.

Jackson, SE, Pearson, NJ, Griffin, WL and Belousova, EA 2004, The application of laser ablation-inductively coupled plasma-mass spectrometry to in situ U/Pb zircon geochronology: Chemical Geology, v. 211, p. 47–69.

Jochum, KP, Nohl, U, Herwig, K, Lammel, E, Stoll, B and Hofmann, AW 2005, GeoReM: A new geochemical database for reference materials and isotopic standards: Geostandards and Geoanalytical Research, v. 29, p. 333–338.

Johnson, TE, Gardiner, NJ, Miljkovic, K, Spencer, CJ, Kirkland, CL, Bland, PA and Smithies, H 2018, An impact melt origin for Earth's oldest known evolved rocks: Nature Geoscience, v. 11, p. 795–799.

Klein, M, Stosch, HG and Seck, HA 1997, Partitioning of high field-strength and rare earth elements between amphibole and quartz-tonalitic melts: an experimental study: Chemical Geology, v. 138, p. 257–271.

Kylander-Clark, ARC, Hacker, BR and Cottle, JM 2013, Laser-ablation split-stream ICP petrochronology: Chemical Geology, v. 345, p. 99–112.

Large, SJE, van Quadt, A, Wotzlaw, J, Guillong, M and Heinrich, CA 2018, Magma evolution leading to porphyry Au–Cu mineralization at the OK Tedi deposit, Papua New Guinea: Trace element geochemistry and high-precision geochronology of igneous zircon: Economic Geology, v. 113, p. 39–61.

Lee, RG, Dilles, JH, Tosdal, RM, Wooden, JL and Mazdab, FK 2017, Magmatic evolution of granodiorite intrusions at the El Salvador porphyry copper deposit, Chile, based on trace element composition and U/Pb age of zircons: Economic Geology, v. 112, p. 245–273.

Lin, S and Beakhouse, GP 2013, Synchronous vertical and horizontal tectonism at late stages of Archean cratonization and genesis of Hemlo gold deposit, Superior Craton, Ontario, Canada: Geology, v. 41, p. 359–362.

Loader, MA, Wilkinson, JJ and Armstrong, RN 2017, The effect of titanite crystallisation on Eu and Ce anomalies in zircon and its implications for the assessment of porphyry Cu deposit fertility: Earth and Planetary Science Letters, v. 472, p. 107–119.

Loucks, RR 2014, Distinctive composition of copper-ore-forming arc magmas: Australian Journal of Earth Sciences, v. 61, p. 5–16.

Loucks, RR, Fiorentini, ML and Rohrlach, BD, 2018, Divergent T-fO2 paths during crystallization of H_2O-rich and H_2O-poor magmas as recorded by Ce and U in zircon, with implications for TitaniQ and TitaniZ geothermometry: Contributions to Mineralogy and Petrology, v. 173, no. 104, doi:org/10.1007/s00410-018-1529-3.

Lu, Y, Fielding, IOH and Wingate, MTD 2019, Introduction to geochronology information 2019, *in* Compilation of geochronology information, 2019: Geological Survey of Western Australia, digital data package, 8p.

Lu, Y, Loucks, RR, Fiorentini, ML, Yang, Z-M and Hou, Z-Q 2015, Fluid flux melting generated post-collisional high-Sr/Y copper-ore-forming water-rich magmas in Tibet: Geology, v. 43, p. 583–586.

Lu, Y, Loucks, RR, Fiorentini, ML, McCuaig, TC, Evans, NJ, Yang, ZM, Hou, ZQ, Kirkland, CL, Parra-Avila, LA and Kobussen, A 2016, Zircon compositions as a pathfinder for porphyry Cu ± Mo ± Au deposits: Society of Economic Geologists Special Publication 19, p. 329–347.

McCuaig, TC, Behn, M, Stein, S, Hagemann, SG, McNaughton, NJ, Cassidy, KF, Champion, DC and Wyborn, LAI 2001, The Boddington gold mine: A new style of Archean Au–Cu deposit, *in* 4th International Archean Symposium, Extended Abstracts *edited by* KF Cassidy, JM Dunphy MJ and Van Kranendonk: AGSO Record 2001/37, p. 453–455.

McCuaig, TC and Hronsky, JMA 2014, The mineral system concept: The key to exploration targeting: Society of Economic Geologists Special Publication 18, p. 153–175.

Moore, G and Carmichael, ISE 1998, The hydrous phase equilibria (to 3 kbar) of an andesite and basaltic andesite from western Mexico: constraints on water content and conditions of phenocryst growth: Contributions to Mineralogy and Petrology, v. 130, p. 304–319.

Moyen, JF and Martin, H 2012, Forty years of TTG research: Lithos, v. 148, p. 312–336.

Mueller, AG, Hall, GC, Nemchin, AA, Stein, HJ, Creaser, RA and Mason, DR 2008, Archean high-Mg monzodiorite–syenite, epidote skarn, and biotite–sericite gold lodes in the Granny Smith–Wallaby district, Australia: U–Pb and Re–Os chronometry of two intrusion-related hydrothermal systems: Mineralium Deposita, v. 43, p. 337–362.

Naney, MT, 1983, Phase equilibria of rock-forming ferromagnesian silicates in granitic systems: American Journal of Science, v. 283, p. 993–1033.

Outhwaite, MD 2018, Metamorphosed Mesoarchean Cu–Mo–Ag mineralization: evidence from the Calingiri deposits, southwest Yilgarn Craton: Geological Survey of Western Australia, Report 183, 216p.

Paton, C, Hellstrom, J, Paul, B, Woodhead, J and Hergt, J 2011, Iolite: Freeware for the visualization and processing of mass spectrometer data: Journal of Analytical Atomic Spectrometry, v. 26, p. 2508–2518.

Pawley, MJ, Wingate, MTD, Kirkland, CL, Wyche, S, Hall, CE, Romano, SS and Doublier, MP 2012, Adding pieces to the puzzle: episodic crustal growth and a new terrane in the northeast Yilgarn Craton, Western Australia: Australian Journal of Earth Sciences, v. 59, p. 603–623.

Percival, JA, Sanborn-Barrie, M, Skulski, T, Stott, GM, Helmstaedt, H and White, DJ 2006, Tectonic evolution of the western Superior Province from NATMAP and Lithoprobe studies: Canadian Journal of Earth Sciences, v. 43, p. 1085–1117.

Reimink, JR, Chacko, T, Stern, RA and Heaman, LM 2014, Earth's earliest evolved crust generated in an Iceland-like setting: Nature Geoscience, v. 7, p. 529–533.

Richards, JP 2011, High Sr/Y arc magmas and porphyry Cu ± Mo ± Au deposits: Just add water: Economic Geology, v. 106, p. 1075–1081.

Rohrlach, BD and Loucks, RR 2005, Multi-million-year cyclic ramp-up of volatiles in a lower crustal magma reservoir trapped below the Tampakan copper–gold deposit by Mio–Pliocene crustal compression in the southern Philippines, *in* Super porphyry copper and gold deposits—a global perspective *edited by* TM Porter: PCG Publishing, Adelaide, v. 2, p. 369–407.

Samperton, KM, Bell, EA, Barboni, M, Keller, CB and Schoene, B 2017, Zircon age–temperature–compositional spectra in plutonic rocks: Geology, v. 45, p. 983–986.

Sano, Y, Terada, K and Fukuoka, T 2002, High mass resolution ion microprobe analysis of rare earth elements in silicate glass, apatite and zircon: lack of matrix dependency: Chemical Geology, v. 184, p. 217–230.

Sillitoe, RH 2010, Porphyry copper systems: Economic Geology, v. 105, p. 3–41.

Sinclair, WD 2007, Porphyry deposits, *in* Mineral Deposits of Canada: A Synthesis of Major Deposit-Types, District Metallogeny, the Evolution of Geological Provinces, and Exploration Methods *edited by* WD Goodfellow: Geological Association of Canada, Mineral Deposits Division, Special Publication no. 5, p. 223–243.

Smythe, DJ and Brenan, JM 2015, Cerium oxidation state in silicate melts: Combined $fO2$, temperature and compositional effects: Geochimica et Cosmochimica Acta, v. 170, p. 173–187.

Smythe, DJ and Brenan, JM 2016, Magmatic oxygen fugacity estimated using zircon–melt partitioning of cerium: Earth and Planetary Science Letters, v. 453, p. 260–266.

Stein, HJ, Barley, ME, Zimmerman, A and Cummins, B 2007, A 3.3 Ga Mo–Cu porphyry-style deposit at Spinifex Ridge, East Pilbara, Western Australia: Re–Os dating of Paleoarchean molybdenite: Goldschmidt Conference Abstract, A970, Goldschmidt 2007, Cologne, Germany, 19–24 August 2007.

Stein, HJ, Hannah, JL, Zimmerman, A, Markey, RJ, Sarkar, SC and Pal, AB 2004, A 2.5 Ga porphyry Cu–Mo–Au deposit at Malanjkhand, central India: implications for Late Archean continental assembly: Precambrian Research, v. 134, p. 189–226.

Stern, RA, Bodorkos, S, Kamo, SL, Hickman, AH and Corfu, F 2009, Measurement of SIMS instrumental mass fractionation of Pb isotopes during zircon dating: Geostandards and Geoanalytical Research, v. 33, p. 145–168.

Sun, S-S and McDonough, WF 1989, Chemical and isotopic systematics of oceanic basalts: implications for mantle compositions and processes, *in* Magmatism In Ocean Basins *edited by* AD Saunders and MJ Norry: Geological Society of London, Special Publicaiton, v. 42, p. 313–345.

Wiedenbeck M, Allé P, Corfu F, Griffin WL, Meier M, Oberli F, von Quadt A, Roddick JC and Spiegel W 1995, Three natural zircon standards for U–Th–Pb, Lu–Hf, trace element and REE analyses: Geostandards Newsletter, v. 19, p. 1–23.

Williamson, BJ, Herrington, RJ and Morris, A 2016, Porphyry copper enrichment linked to excess aluminium in plagioclase: Nature Geoscience, v. 9, p. 237–241.

Witt, W, Cassidy, K, Lu, Y-J and Hagemann, S 2018, Syenitic group intrusions of the Archean Kurnalpi Terrane, Yilgarn Craton: Hosts to ancient alkali porphyry gold deposits?: Ore Geology Reviews, v. 96, p. 262–268.

This Report presents the results of the first craton-wide study to systematically examine zircons from granitic rocks in the Archean Yilgarn Craton as potential metallogenic fertility indicators of Archean magmatic–hydrothermal systems. The fertile granitic rocks from the Calingiri Cu–Mo and Boddington Au–Cu–Mo deposits in the Yilgarn Craton show distinctly higher zircon Eu anomaly values (Eu/Eu*>0.4), which are mainly due to amphibole-dominated fractionation in hydrous melts, similar to Phanerozoic fertile granitic rocks. By contrast, the barren granitic rocks from across the Yilgarn Craton display lower zircon Eu/Eu* values (Eu/Eu*<0.4) and plagioclase-dominated fractionation. These results suggest that the zircon Eu anomaly and trace element ratios can be used to distinguish fertile from barren granitic rocks in Archean and Phanerozoic terranes, providing an effective geochemical exploration tool to assess the metallogenic fertility of granitic rocks over geological time.

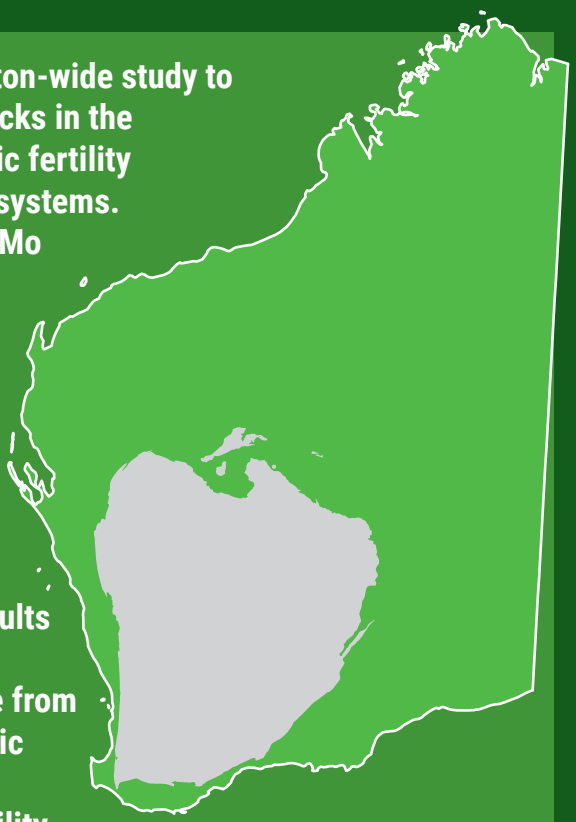

Further details of geoscience products are available from:

Information Centre
Department of Mines, Industry Regulation and Safety
100 Plain Street
EAST PERTH WA 6004
Phone: (08) 9222 3459 Fax: (08) 9222 3444

www.dmp.wa.gov.au/GSWApublications

LU et al.

ZIRCON FINGERPRINTING OF MAGMATIC–HYDROTHERMAL SYSTEMS IN THE ARCHEAN YILGARN CRATON

REPORT 197